공학석사학위논문

Data-driven damping evaluation of cable-supported bridges from long-term data

장기 데이터를 통한 케이블 교량의 데이터 주도적 감쇠 평가

2020년 2월

서울대학교 대학원

건설환경공학부

황도연

Abstract

This thesis presents a data-driven damping evaluation process for long-span cable-supported bridges, whose low damping capacity and flexibility make damping a critical factor in assessing their vibrational serviceability. While many studies have focused on improvement of damping estimation and evaluation from relatively short-term data, there are many questions about variability of damping in changing environmental conditions. Long-term operational data collected from built-in monitoring systems of two cable-supported bridges were acquired for this study. An automated damping estimation process using a density-based clustering algorithm, based on Natural Excitation Technique – Eigensystem Realization Algorithm (NExT-ERA) was developed and employed. Amplitude dependency of damping ratios was observed, as well as effects from aerodynamic phenomena. After evaluating damping ratios with environmental conditions in context, statistical models were presented. It is recommended that similar damping evaluation processes be carried out for other cable-supported bridges to construct a damping database that can be used to gain a better understanding of damping.

Keywords: automated modal analysis, cable-supported bridges, damping, long-term data, NExT-ERA

Student Number: 2018-22388

Table of Contents

List of Figures

List of Tables

1. Introduction

1.1. Research Background

Damping is associated with the energy dissipation of a system in motion. It is represented by a dimensionless measure called the damping ratio, or fraction of critical damping.[1] In structural engineering fields, damping ratios are used for aerodynamic and aeroelastic analysis, bridge-vehicle interaction analysis, finite element model updating and other dynamic analyses. For structures such as long-span cable-supported bridges that are relatively more flexible and possess low structural damping capacity, damping ratios are especially critical in evaluation of vibrational serviceability.

Current code practices in Korea suggests 0.4% of structural damping ratio for welded steel cable-stayed / suspension bridges (Table 1.1) according to Commentary on Highway Bridge Design Code [2]. However, damping capacity cannot be predicted before design and completion of structure, and thus may be lower than the initially assumed values specified in code.

Table 1.1. Suggested structural damping ratios in current practices [2]

Structural Type			Structural Damping Ratio (%)
Cable-stayed/ suspension bridges	Steel bridges	Welded	0.4
		High resistance bolts	0.5
		Ordinary bolts	0.8
	Composite bridges		0.6
	Concrete bridges		0.8
Independent pylons	Steel		0.2
	Concrete		0.5

This issue is highlighted by recent occurrences of vortex induced vibrations (VIV) in multiple cable-supported bridges in Korea that caused undesirable vibrations exceeding serviceability limits. In the case of the Second Jindo Bridge, it was discovered by Kim et al. [3] that one of the major causes of such undesirable vibrations was lower damping ratios (0.29% for the 1st vertical mode) than initially assumed design values. Similar cases were observed and examined for the Yi Sun Shin bridge [4], [5] and Cheonsa Bridge, where it was concluded that lower damping capacity was one of the causes for their serviceability issues. These recent events underscore the importance of damping estimation after construction of bridges, as outlined in many previous literatures.

The simplest approach to identifying the damping ratios of structures is through controlled dynamic testing. This is generally referred to as experimental modal analysis (EMA), in which dynamic properties of a structure (modal frequencies, shapes and damping ratios) are identified from measurements of excitation and response.[6] While EMA can be readily applied to small structures that are in controlled environments, it is quite a challenge for large civil engineering structures such as bridges. These structures are large and massive, requiring specialized equipment such as mechanical exciters that are costly and cumbersome. Furthermore, bridges are subjected to a multitude of uncontrollable excitation sources such as wind and traffic, rendering a controlled experiment nearly impossible. Consequently, recent studies have focused on operational modal analysis (OMA), in which dynamic properties are identified from output only. OMA makes use of ambient excitation sources such as wind and traffic that are already present during operational conditions and allows civil engineers to identify dynamic properties during operation of structures; only response data such as acceleration and displacement are required. With more availability of built-in monitoring systems for bridges, operational field data can be used in conjunction with OMA to perform damping estimation that reflects environmental conditions.

However, there are major challenges in applying OMA for damping estimation. Because OMA is a type of system identification problem, it is ill-posed and thus highly sensitive to parameter selection. Nonstationarity of excitation and response is also an issue, since it violates one of the fundamental assumptions of OMA. Variability of damping itself creates difficulties since there is no single well-established damping mechanism, and it is well-known that damping varies by many environmental conditions. All of the aforementioned issues contribute to the uncertainties of damping ratios and makes OMA-based damping estimation a difficult process.

1.2. Literature Survey

In order to identify environmental effects on the modal properties, Soyoz et al. [7] used long-term monitoring data collected over a 5-year period to estimate modal frequencies of a concrete bridge. Mao et al. [8] performed automated modal identification with k-means clustering and other classification techniques on 20 days of data collected from the structural health monitoring (SHM) system of Sutong cable-stayed Bridge and analyzed the environmental effects and variations in modal frequencies. However, for both studies, only modal frequencies, not damping ratios, were identified from the long-term data.

Asadollahai and Li [9] performed statistical analysis of modal properties from long-term data collected by a wireless sensor network over a 1-year period and examined the effects of temperature and excitation levels on modal properties including damping ratios. Zhang Yilan et al.[10] also assessed the effects of environmental conditions on modal properties from data collected by a long-term monitoring system. For both studies however, environmental effects were unclear due to large uncertainties in estimated damping ratios.

To increase robustness of damping estimation process, Kim et al. [11] performed

parametric studies on a time domain OMA algorithm and successfully estimated damping ratios for a cable-stayed bridge from 4 days of operational field measurement data. Boroschek and Bilbao [12] applied Ordering Points to Identify the Clustering Structure (OPTICS), a type of density-based clustering algorithm, to automatically cluster data and remove spurious poles from OMA results. Kim et al. [13] applied displacement reconstruction to measured acceleration and demonstrated that using the reconstructed displacement physically repressed high-frequency components from traffic-induced vibrations and enhanced the stability of damping estimates.

1.3. Research Scope and General Layout

This dissertation seeks to first, propose an automated damping estimation process that requires minimum user intervention and is robust against faulty data. Second, by applying the proposed process to long-term operational data obtained from monitoring systems of two cable-supported bridges, it aims to construct statistical models of damping ratios and assess the effects of environmental conditions.

1.3.1. Target Structures

Jindo Bridge (the First Jindo Bridge) and Sorok Bridge were selected as target structures for damping estimation. Both bridges are located at the southern part of the Korean peninsula, in the South Jeolla Province (Jeollanam-do). Their general characteristics are outlined in Table 1.2.

Table 1.2. General characteristics of target structures

Bridge	Jindo Bridge	Sorok Bridge
Structure Type	Cable-stayed bridge	Self-anchored suspension bridge
Main Span Length	344 m	250 m
Deck Type	Steel-box girder	Steel-box girder
Pylon Type	Steel pylon	Diamond concrete pylon
Cable Type	Locked Coil Rope (LCR)	Mono-cable, Prefabricated Parallel Wire Strand (PPWS) cable

(a)

(b)

Figure 1.1. Target structures (a) Jindo Bridge; (b) Sorok Bridge

Monitoring systems built into the target structures are maintained by the Korea Infrastructure Safety Corporation (KISTEC). Long-term data were directly acquired from the servers of the monitoring systems with permission from KISTEC. An overview of the available sensors and data characteristics for each of the target structures is outlined in Table 1.3. For Sorok Bridge, only two accelerometers at the midspan were utilized as the accelerometers at 1/4 span were often corrupted with faulty data or did not match the modal frequencies detected at midspan.

Table 1.3. Available sensors and data characteristics for target structures

Bridge	Jindo Bridge	Sorok Bridge
Accelerometer	Total: 2 (2 at 1/2 points of the main span)	Total: 4 (2 at 1/4, 2 at 1/2 points of the main span)
Anemometer	1 propeller type and 1 ultrasonic type at midspan	1 propeller type at midspan
Acquired Data	2016-01-01 00:00 ~ 2018-08-31 23:00	2015-01-27 17:00 ~ 2019-04-05 11:00
Sampling Frequency	100 Hz	100 Hz
Data Format	10-minute segments, TXT files	10-minute segments, TXT files

1.3.2. General Layout

Chapter 2 describes in detail the proposed automated damping estimation process. Threshold-based fault isolation and displacement reconstruction are used for preprocessing the measured acceleration data. A time domain OMA algorithm is used for damping estimation and postprocessing is performed with a density-based clustering algorithm. In Chapter 3, results from application of the proposed process are discussed, particularly in relation to environmental conditions. Finally, damping ratios are evaluated and statistical models are presented for each target structure.

2. Automated Damping Estimation Process

2.1. Preprocessing

Before damping estimation, data from measurement systems must be preprocessed beforehand in order to isolate various faults. Such faults, if not properly removed, can lead to failure of damping estimation process or erroneous results.

2.1.1. Threshold-based Fault Isolation

Various types of faults inevitably exist in measurement data acquired from long-term monitoring systems. Such faults include missing values, bias, drift, gain and noise. While missing values, bias and drift can be easily detected prior to analysis from simple data inspection (e.g. checking for not a number (NaN) values) and time domain data statistics (e.g. mean and root mean square (RMS) values), noise cannot be so easily isolated from cursory inspection. Examples of faults found in long-term data are included in Figure 2.1.

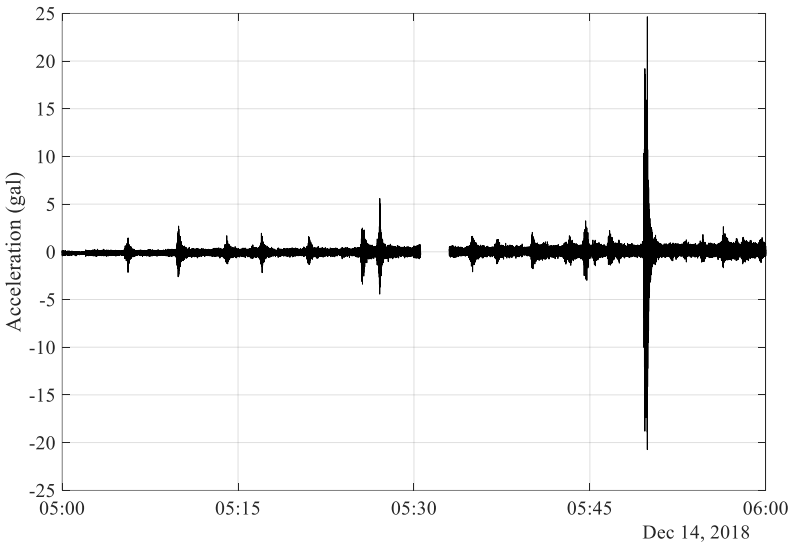
25
20
15
10
5
0
-5
-10
-15
-20
-25
Acceleration (gal)
05:00
05:15
05:30
05:45
06:00
Dec 14, 2018

(a)

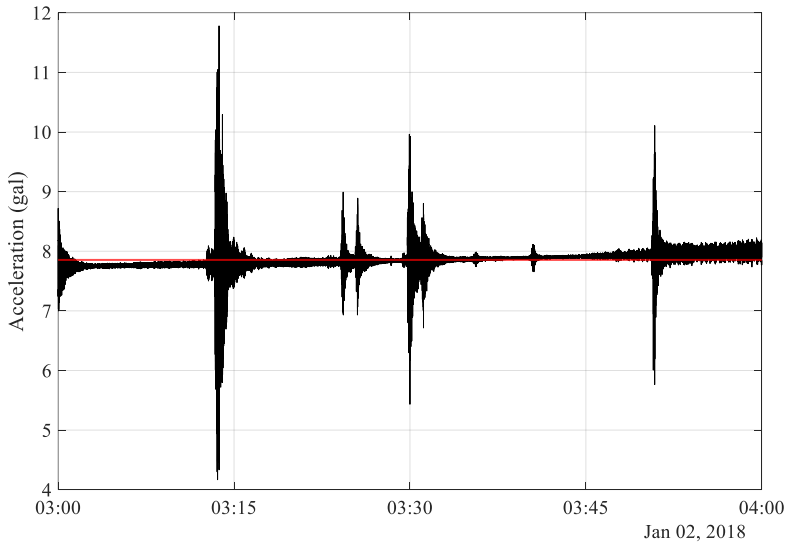
12
11
10
9
8
7
6
5
4
Acceleration (gal)
03:00
03:15
03:30
03:45
04:00
Jan 02, 2018

(b)

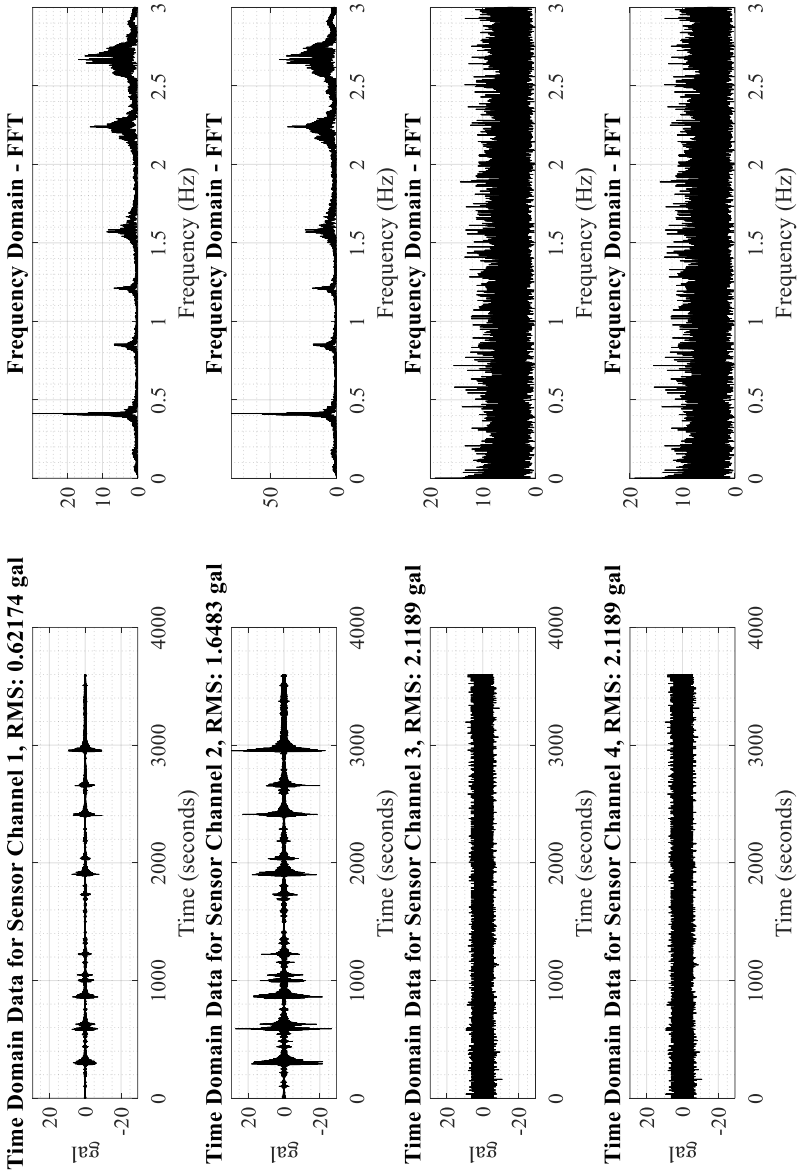

(c)

Figure 2.1. Examples of faulty data found in long-term data: (a) Missing values; (b) Bias and drift; (c) Unidentified noise

Thus, maximum correlation factor (MCF), a simple measure representing similarity of signals in the frequency domain is applied for isolation of faulty data. MCF is defined in Equation (2.1),

$$MCF(i) = max\big(Corr(P_i)\big) \cdot 100 \tag{2.1}$$

where P_i is the power spectral density of the signal in channel i, $Corr$ is the matrix of pairwise correlation coefficients for all channels, and MCF is the maximum value of the resulting matrix rows excluding its diagonal terms. Thus, if a channel possesses a relatively low MCF value, it will imply dissimilarity compared to other channels in the frequency domain. Another point to consider is that if a channel possesses an MCF value of exactly 100%, it suggests that the channel is comprised of noise identical to another channel comprised of the same noise. MCF values for long-term data obtained from target structures were calculated and manually inspected. It was assessed that datasets with MCF values below 80% indicated the presence of abnormal channels. Such an example is shown below in Figure 2.2. By employing MCF to long-term data, faulty data can be isolated with minimum user intervention and computational overhead is reduced that would otherwise have been wasted on defective data.

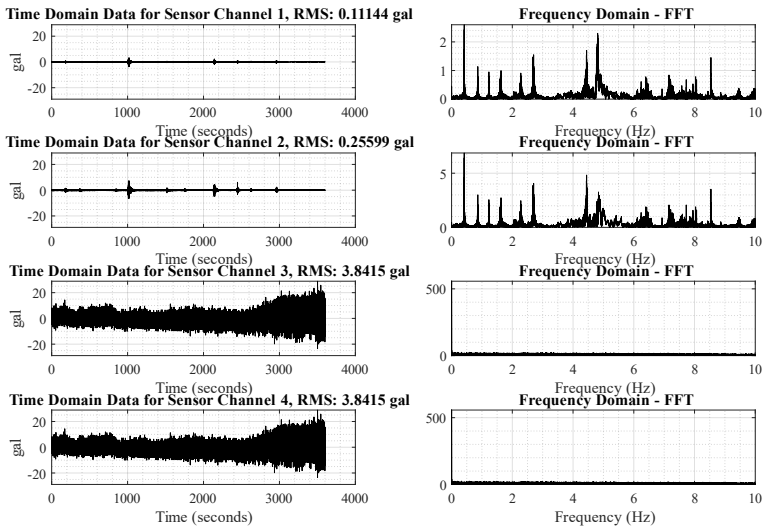

(a)

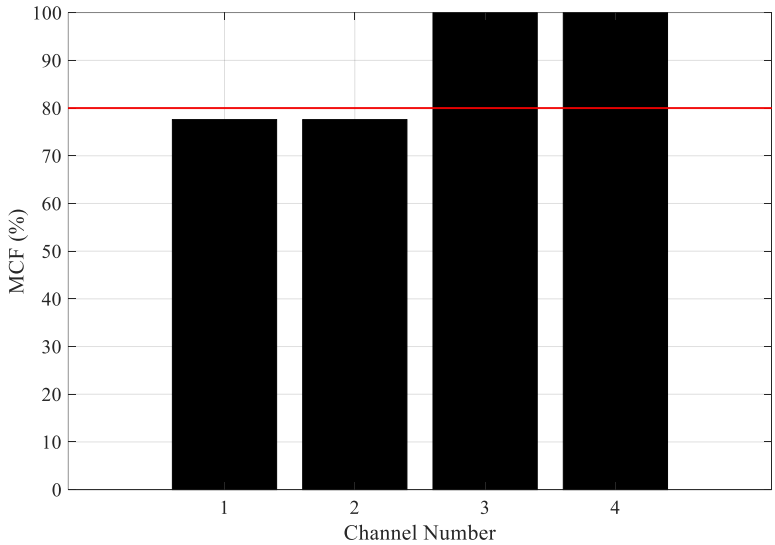

(b)

Figure 2.2. Example of isolated faulty data, 2015-03-13 19:00 at Sorok Bridge (a) acceleration in time and frequency domain; (b) MCF values for channels

2.1.2. Displacement Reconstruction

One of the many challenges of OMA-based damping estimation is non-stationarity of response. Kim et al. [13] has already demonstrated that applying displacement reconstruction to measured acceleration improves stability and robustness of damping estimation. Hence, displacement reconstruction is applied to the acquired acceleration data with the same parameters suggested in Hong et al. [14], detailed in Table 2.1. Figure 2.3 shows the reconstructed displacement in both time and frequency domain.

Table 2.1. Parameters used for displacement reconstruction

Parameters	Values, Options
Target accuracy	0.97
Target frequency	*Automatically select lowest modal frequency by peak-picking from PSD*
Time-window size	Long

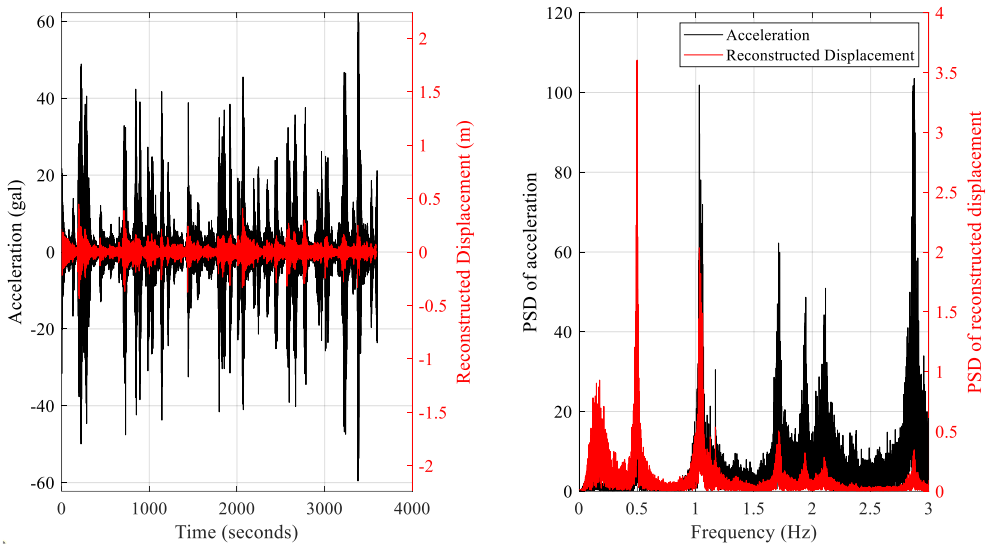

Figure 2.3. Reconstructed displacement in time and frequency domain

It can be observed that the reconstructed displacement suppresses high-frequency components, while still preserving the peaks of structural modes. It is shown later in that this enables the reduction of required model order for stable damping estimates and easier removal of spurious poles during postprocessing.

2.2. Damping Estimation

2.2.1. Natural Excitation Technique (NExT)

NExT was introduced by James et al. [15] for OMA and has been used successfully for many modal analysis applications. When the assumption that the excitation and response are weakly stationary processes is satisfied, the cross-correlation function between the measurement response vector and the reference response vector satisfies the homogeneous equation of motion, i.e. it has the characteristics of an impulse response function (IRF). A brief description of the process is presented below. [16]

Equation (2.2) describes the forced vibration of an n degree-of-freedom (DOF)

linear, time-invariant system.

$$M\ddot{x}(t) + C\dot{x}(t) + Kx(t) = f(t) \tag{2.2}$$

where $x(t)$ and $f(t)$ are $n \times 1$ displacement and excitation vectors while M, C, K are $n \times n$ mass, damping and stiffness matrices. For the case where excitation and response are weakly stationary processes, Equation (2.2) can be rewritten as,

$$\begin{aligned} &M\mathrm{E}\left[\ddot{X}(t)X_{ref}(t-\tau)\right] + C\mathrm{E}\left[\dot{X}(t)X_{ref}(t-\tau)\right] \\ &+K\mathrm{E}\left[\mathrm{X}(t)X_{ref}(t-\tau)\right] = E[F(t)X_{ref}(t-\tau) \end{aligned} \tag{2.3}$$

where $X, \dot{X}, \ddot{X}$ and F are displacement, velocity, acceleration and excitation vectors while $E[\,]$ denotes the expectation. Because of the assumption that excitation and response are weakly stationary processes, they are uncorrelated. Thus, the term $R_{X_{ref}F}(\tau) = 0$. Going further, as presented by Bendat and Piersol [17],

$$\mathrm{R}_{\mathrm{X}_{\mathrm{ref}}\dot{X}}(\tau) = \dot{R}_{X_{ref}X}(\tau) \tag{2.4}$$

$$\mathrm{R}_{\mathrm{X}_{\mathrm{ref}}\ddot{X}}(\tau) = \ddot{R}_{X_{ref}X}(\tau) \tag{2.5}$$

Combining the above derivations and rewriting Equation (2.3),

$$M\ddot{\mathbf{R}}_{X_{ref}X}(\tau) + C\dot{\boldsymbol{R}}_{X_{ref}X}(\tau) + K\boldsymbol{R}_{X_{ref}X}(\tau) = \mathbf{0} \tag{2.6}$$

Thus, Equation (2.6) shows that the cross-correlation function between the displacement of measurement vector and the response vector satisfies the free vibration equation of motion. Similarly, it can be shown that the same is satisfied for acceleration.

Because the final cycles of the calculated IRF can be unstable, only some of the

initial cycles of IRF were used for the next steps of the analysis.[6] In this dissertation, only the first cycles of the IRF whose amplitude reached 70% from the initial stable amplitude were used, as illustrated in Figure 2.4.

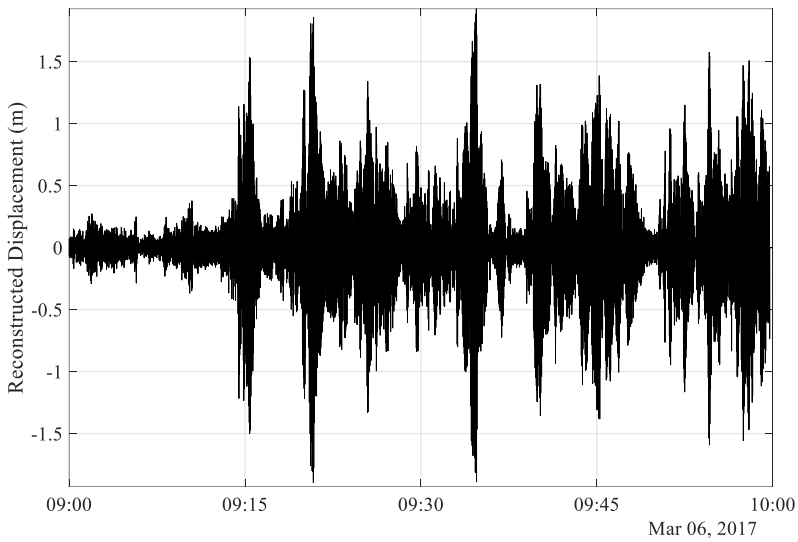

(a)

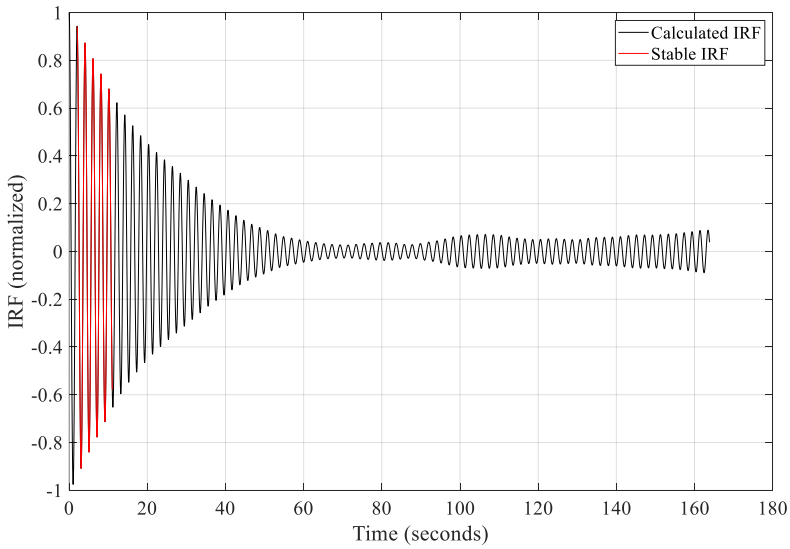

(b)

Figure 2.4. IRF calculated from reconstructed displacement (a) reconstructed displacement; (b) calculated normalized IRF

Three parameters are required for the NExT procedure. Number of FFTs for calculation of cross-correlation function, data length and length of IRF to use be used later (i.e. size of Hankel matrices). Because parametric studies for NExT were already performed in detail for similar structures, [18], [19] the suggested parameters were applied in the same manner in this dissertation.

2.2.2. Eigensystem Realization Algorithm (ERA)

ERA is a modal identification technique proposed by Juang and Pappa [20] that can calculate the system matrices from the impulse response function. Again, a brief description of the technique presented below.

The first step in ERA is to construct Hankel matrices as defined in Equation (2.7).

$$\mathbf{H}(k-1) = \begin{bmatrix} \mathbf{Y}(k) & \cdots & \mathbf{Y}(k+p) \\ \vdots & \ddots & \vdots \\ \mathbf{Y}(k+r) & \cdots & \mathbf{Y}(k+p+r) \end{bmatrix} \tag{2.7}$$

$$\mathbf{Y}(k) = \begin{bmatrix} y_{1,1}(k) & \cdots & y_{1,m}(k) \\ \vdots & \ddots & \vdots \\ y_{n,1}(k) & \cdots & y_{n,m}(k) \end{bmatrix} \tag{2.8}$$

where n and m are number of measurement and reference channels and r and p are number of block rows and columns. $Y(k)$ is an $n \times m$ matrix of the cross-correlation function at discrete time step k, defined in Equation (2.8).

The constructed Hankel matrix for $k = 1$ is decomposed using singular value decomposition (SVD),

$$\mathbf{H}(\mathbf{0}) = \mathbf{PDQ}^{\mathbf{T}} = [\mathbf{P_1} \quad \mathbf{P_2}] \begin{bmatrix} \mathbf{D_1} & \mathbf{0} \\ \mathbf{0} & \mathbf{0} \end{bmatrix} \begin{bmatrix} \mathbf{Q_1^T} \\ \mathbf{Q_2^T} \end{bmatrix} = \mathbf{P_1 D_1 Q_1^T} \tag{2.9}$$

where $\mathbf{D}$ is a diagonal matrix of monotonically increasing singular values and $\mathbf{D_1}$ is an $N \times N$ $(N \leq p)$ diagonal matrix truncated by model order N. $\mathbf{P_1}$ and $\mathbf{Q_1}$ are

$n(r+1) \times N$ and $m(p+1) \times N$ matrices that are the first N columns of the **P** and **Q** matrices.

Using the matrices derived so far, discrete time state-space realization matrices can be calculated with the following equations,

$$\widehat{\mathbf{A}} = \mathbf{D_1}^{-\frac{1}{2}}\mathbf{P_1^T}\mathbf{H(1)}\mathbf{Q_1}\mathbf{D_1}^{-\frac{1}{2}} \tag{2.10}$$

$$\hat{\mathbf{C}} = \mathbf{E_m^T}\mathbf{P_1}\mathbf{D_1^{\frac{1}{2}}} \tag{2.11}$$

where $E_m^T = [\mathbf{I}\ \mathbf{0}]$, is used to select the system matrix $\hat{\mathbf{C}}$.

To transform the discrete-time realization to the continuous-time domain, an eigenvalue problem for $\widehat{\mathbf{A}}$ is considered in Equation (2.12).

$$\widehat{\mathbf{A}} = \widehat{\mathbf{\Psi}}\widehat{\mathbf{\Lambda}}\widehat{\mathbf{\Psi}}^{-1} \tag{2.12}$$

Where, $\widehat{\mathbf{\Lambda}}$ and $\widehat{\mathbf{\Psi}}$ are the eigenvalue and eigenvector matrices. The natural frequencies f_i, damping ratios ξ_i and mode shapes $\widehat{\mathbf{\Phi_i}}$ can be calculated by the following equations.

$$\begin{aligned} f_i &= \frac{\omega_i}{2\pi} = \frac{\sqrt{\sigma_i^2 + \Omega_i^2}}{2\pi} \\ \xi_i &= -\cos\left[\tan^{-1}\left(\frac{\Omega_i}{\sigma_i}\right)\right] \\ \widehat{\mathbf{\Phi}_i} &= \hat{\mathbf{C}}\widehat{\mathbf{\Psi}}_i \end{aligned} \tag{2.13}$$

$$\widehat{\mathbf{\Lambda}} = diag(\overline{\sigma_i} \pm j\overline{\Omega}_i)$$

$$\sigma_i \pm j\Omega_i = \frac{\ln(\overline{\sigma_i})}{\Delta t} \pm j\frac{\ln(\overline{\Omega}_i)}{\Delta t} \tag{2.14}$$

In Equation (2.14), Δt is the sampling period, or discrete time step of the measured data.

The results of ERA can be easily visualized by a stabilization diagram, a tool frequently used in the OMA community to identify the correct number of poles, or model order for ERA. Stables poles remain constant for all or most of the iterations of model order, while spurious poles behave erratically. A stabilization diagram will be presented in Chapter 2.3.1, along with hard validation criteria to filter out spurious poles.

2.2.3. Modal Accuracy Indicators

In order to identify spurious poles, two modal accuracy indicators were calculated in the ERA process. Extended Modal Amplitude Coherence (EMAC) and Consistent Mode Indicator (CMI) were calculated according to the procedure detailed in literature. [21]. EMAC is a measure of how accurately a mode projects forward onto the impulse response data and CMI is an improved consistency indicator that is calculated by Equation (2.15),

$$\mathrm{CMI_i} = \mathrm{EMAC_i} \cdot \mathrm{MPC_i} \tag{2.15}$$

where MPC refers to Modal Phase Collinearity, a measure that quantifies the spatial consistency of modes. Because detailed derivations of modal accuracy indicators have already been sufficiently described in the references cited above, they were not repeated within this dissertation.

2.2.4. Parameters Applied for NExT-ERA

Most of the parameters and procedure for NExT-ERA applied in this dissertation

follow the recommendations from previous literature [18], [19]. One key difference is that in this dissertation, a multi-channel NExT-ERA, commonly referred to as MNExT-ERA was applied instead of single-channel NExT-ERA. Therefore, while the overall procedure for NExT-ERA is similar, several modifications were made. First, when calculating the cut-off point for the impulse response functions from NExT to use in the Hankel matrices, the minimum stable point was calculated by the maximum value for all channels. Second, when constructing the Hankel matrices, the size of the matrices was $n(r+1) \times m(p+1)$ instead of $(r+1) \times (p+1)$ since multiple reference and measurement channels were taken into consideration. Lastly, a relatively low model order of 20 was selected for ERA as displacement reconstruction during preprocessing allowed stable damping estimation with lower model orders. Table 2.2 summarizes the parameters used in NExT-ERA.

Table 2.2. Parameters used for NExT-ERA

Parameter	Values, Options
Number of FFT	2^{15}
Data Length	1 hour
Size of Hankel Matrices	*Automatically calculated by NExT*
System Order	20

2.3. Postprocessing

2.3.1. Hard Validation

To exclude spurious poles in ERA results, multiple hard validation criteria are applied in postprocessing. First, poles with modal frequencies below 0 Hz or exceeding 3 Hz were removed since the interested structural modal frequencies of the target structures are exist below 3 Hz. Second, poles with modal damping ratios below 0% or those exceeding 5% were removed, as both target structures are long-span cable-supported bridges with relatively low damping capacity.[22] Poles with

EMAC values lower than 99% and CMI values under 80% were also removed, in accordance with previous studies. [4], [16] The applied hard validation criterion are summarized in Table 2.3, and the resulting stabilization diagrams are presented in Figure 2.5.

Table 2.3. Applied hard validation criteria

Criteria	Values, Ranges
Modal Frequencies f_i	$0\ \mathrm{Hz} < \mathrm{f_i} < 3\ \mathrm{Hz}$
Modal Damping Ratios ξ_i	$0\% < \xi_\mathrm{i} < 5\%$
EMAC	$\mathrm{EMAC_i} > 99\%$
CMI	$\mathrm{CMI_i} > 80\%$

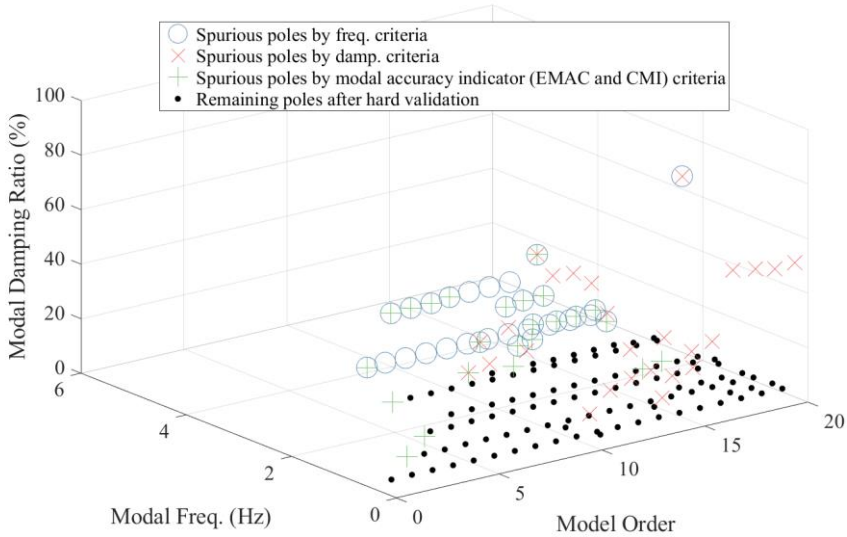

(a)

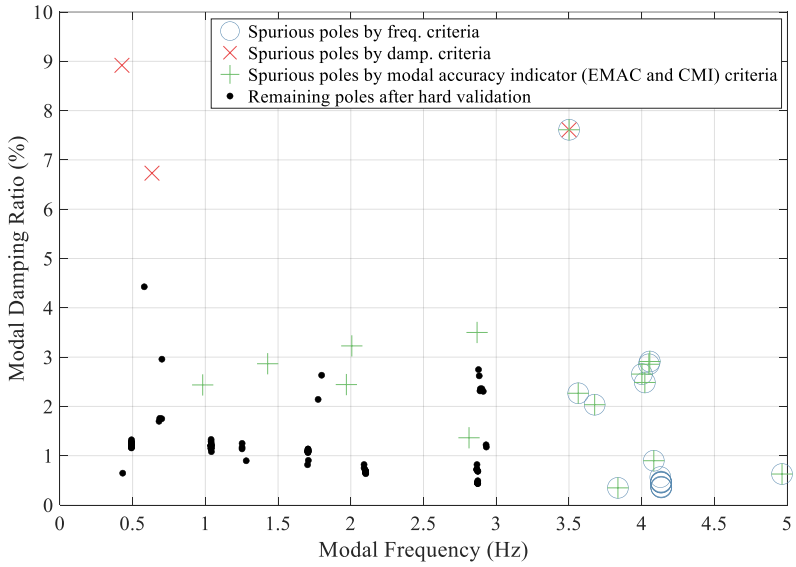

(b)

Figure 2.5. Stabilization diagrams with application of hard validation criteria, data from Jindo Bridge at 2017-03-06 09:00

2.3.2. Density-Based Clustering

Even after hard validation, spurious poles may still exist in the stabilization diagram. To separate the remaining spurious poles from physical poles and automatically identify modal parameters of the target structure, a density-based clustering algorithm is applied to the data.

Previous studies have applied clustering methods such as hierarchical clustering and k-means clustering after hard validation to automatically identify modal parameters. However, multiple drawbacks exist for the two methods in application to OMA. The first drawback for hierarchical clustering and k-means clustering is that they require decision making on where to cut the dendrogram and the number of clusters, respectively. Because some structural modes may not be sufficiently excited depending on varying environmental conditions, applying classification methods based on a predefined number of clusters will result in erroneous classifications. This requires the user to develop additional processes to dynamically calculate cut locations or number of clusters for each dataset, a challenging task that reduces the robustness of the algorithm. Second, for standard k-means clustering, using other distance measures than the Euclidean distance may stop the algorithm from converging, resulting in a less stable process. This is a significant limitation when attempting to incorporate modal similarity measures such as Modal Assurance Criterion (MAC) into the definition of distance between poles.

To overcome such difficulties, density-based spatial clustering of application with noise (DBSCAN) [23], a type of density-based clustering algorithm is used in this study. DBSCAN requires two parameters: ϵ, the neighborhood search radius and *minPts*, the minimum number of points required for a core point. The overall steps of DBSCAN are introduced below, as implemented in MATLAB.[24]

1. From the input dataset, an observation, or point, is selected and initialized as the first cluster, labeled as 1.

2. A set of points within the neighborhood search radius ϵ are found. If the number of neighbors exceeds *minPts*, the current point is classified as a core point belonging to cluster 1. If the number of neighbors does not exceed *minPts*, the current point is labeled as an outlier, or noise point, belonging to cluster -1. Continue to step 4 in this case.

3. Iterate for each neighbor until there are no new neighbor points are found that can be classified as cluster 1.

4. Select a new point and increase the cluster count by 1.

5. Repeat the steps outlined in steps 2~4 until all points in the dataset are labeled.

If two clusters with varying densities have border points with distance less than ϵ, DBSCAN merges the two clusters into one.

There are many advantages to DBSCAN, chief among them being that there is no need to specify the number of clusters beforehand unlike k-means clustering. Precomputed distances between points other than Euclidean distances may also be used, allowing applications to data with higher dimensions and custom distance measures. Finally, because the concept of noise is built into DBSCAN, it is robust against outliers, which exist in the form of spurious poles in stabilization diagrams for OMA applications.

In this dissertation, a non-dimensional modal similarity distance measure between poles *i* and *j* is defined in Equation (2.16), denoted as $\mathrm{d_{i,j}}$.

$$\mathrm{d_{i,j}} = \frac{|f_i - f_j|}{f_i} + \frac{|\xi_i - \xi_j|}{\xi_i} + 1 - \mathrm{MAC}_{ij} \tag{2.16}$$

Where, f_i, f_j and ξ_i, ξ_j are modal frequencies and damping ratios of poles i and j and MAC_{ij} denotes the MAC value between poles i and j. MAC is a modal shape similarity measure defined by Equation (2.17),

$$\mathrm{MAC}_{i,j} = \frac{\left|\widehat{\Phi}_i^H \widehat{\Phi}_j\right|^2}{\left(\widehat{\Phi}_i^H \widehat{\Phi}_i\right)\left(\widehat{\Phi}_j^H \widehat{\Phi}_j\right)} \tag{2.17}$$

where the superscript H denotes the Hermitian of a matrix. If a modal shape is not available, $\mathrm{MAC}_{i,j}$ is assumed to have a value of 1 for all poles, essentially removing MAC from the distance definition.

Parametric studies using actual measurement data were performed in order to select the appropriate parameters for DBSCAN.

Neighborhood search radius ϵ must be large enough to sufficiently encompass a physical mode cluster, while smaller than the border distance between clusters. Because the modal frequencies of the target structures are already known values, a certain minimum threshold for ϵ can be calculated based on the interested modal frequencies.

Table 2.4. Interested modal frequencies for target structures

Mode	Modal Frequencies (Hz)	
	Jindo Bridge	**Sorok Bridge**
1st Vertical	0.495	0.412
3rd Vertical	1.034	0.849
5th Vertical	1.699	1.210

Calculating all the hypothetical core distances between physical mode clusters according to Equation (2.16) reveals that ϵ must be smaller than 0.298. This is to ensure that no two modes are merged into one cluster, since the calculated value is for the core distance, not border distance. Even though damping and MAC terms in the distance equation may allow some leeway, keeping ϵ below the calculated

minimum value would be beneficial for robustness, as modal frequencies fluctuate depending on environmental conditions.

Minimum number of points required for a core point *minPts*, must be large enough to ignore spurious poles but small enough to capture poles of weakly excited structural modes. In general applications of DBSCAN it is recommended that $minPts$ be at least $2 \cdot dim$, where dim is the number of dimensions in the data set.[25] It is also noted that larger values are suggested for large, noisy or data with duplicates.[26] Previous literature using similar methodology [12] suggested that 1/3 of the total number of model orders be set for *minPts*. In this application, the number of dimensions is 2, 3 if MAC is included in the distance. With a model order of 20, the initial optimal *minPts* is then calculated to be 6.

After performing DBSCAN with varying ϵ, it can be observed that while smaller ϵ values are able to better separate clusters, there are no benefits for smaller values beyond $\epsilon = 0.1$. In fact, DBSCAN begins to fail to recognize physical clusters with lower densities with values smaller than 0.1. (Figure 2.6, Table 2.5) Thus, an ϵ value of 0.1 was selected.

Varying *minPts* had little impact on the final modal damping ratio results (Table 2.6), but clusters comprised of spurious poles were identified from *minPts* with values lower than 6 (Figure 2.7 (a)). Thus, a *minPts* value of 6 was selected. Note that for all figures and tables from here on, "V" prefix refers to "vertical mode."

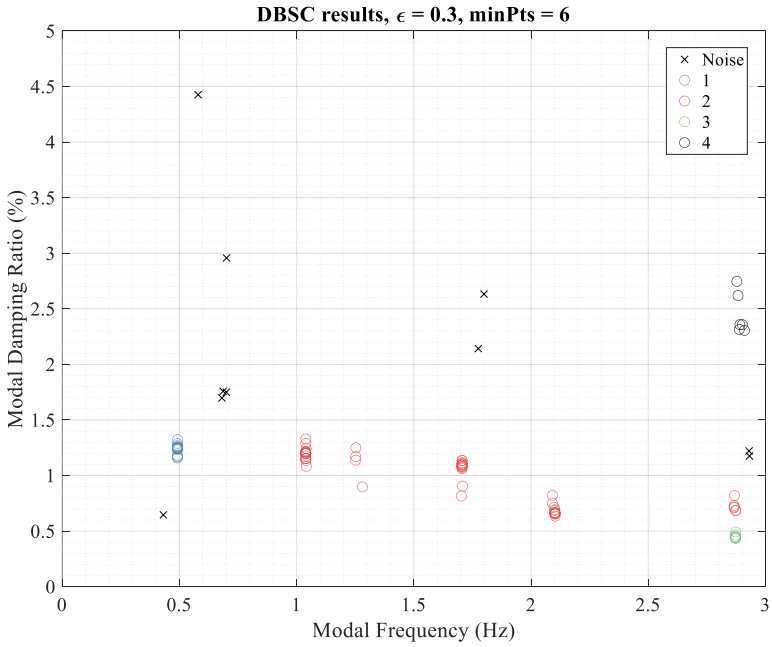
DBSC results, ϵ = 0.3, minPts = 6
Noise
1
2
3
4
Modal Damping Ratio (%)
Modal Frequency (Hz)
0
0.5
1
1.5
2
2.5
3
3.5
4
4.5
5

(a)

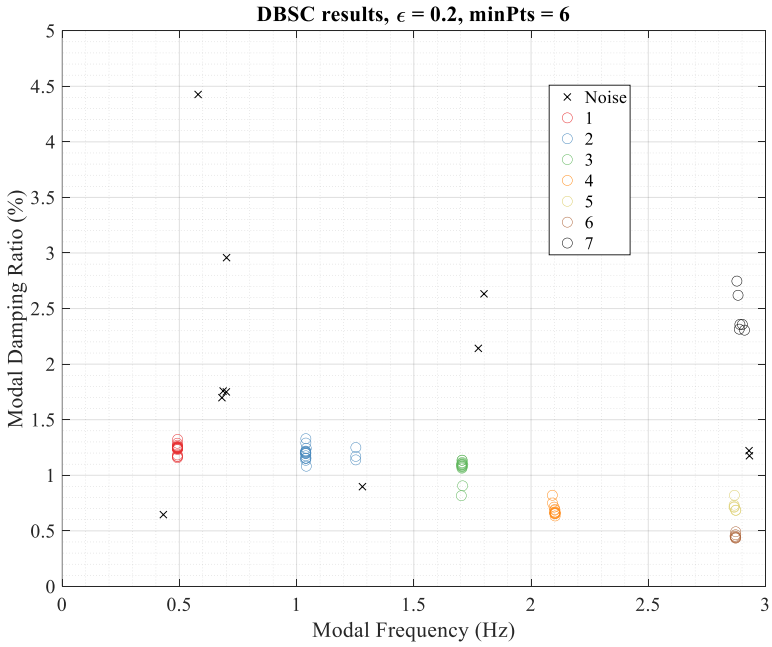
DBSC results, ϵ = 0.2, minPts = 6
Noise
1
2
3
4
5
6
7
Modal Damping Ratio (%)
Modal Frequency (Hz)
0
0.5
1
1.5
2
2.5
3
3.5
4
4.5
5

(b)

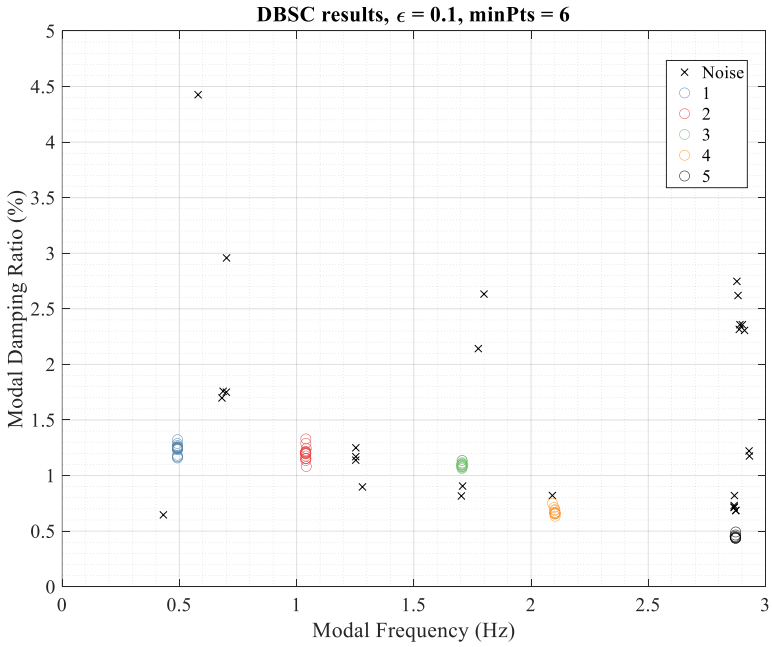
DBSC results, ϵ = 0.1, minPts = 6
Modal Damping Ratio (%)
Modal Frequency (Hz)
Noise
1
2
3
4
5

(c)

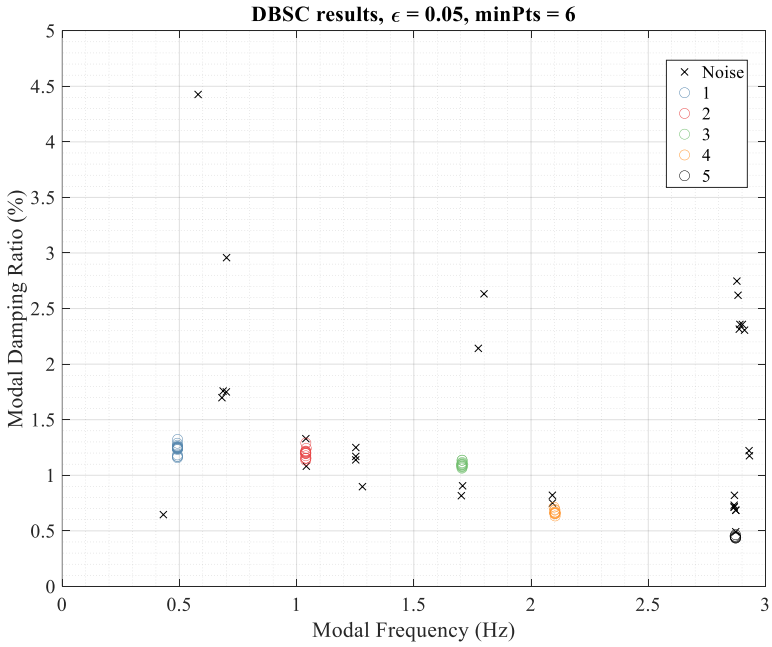
DBSC results, ϵ = 0.05, minPts = 6
Modal Damping Ratio (%)
Modal Frequency (Hz)
Noise
1
2
3
4
5

(d)

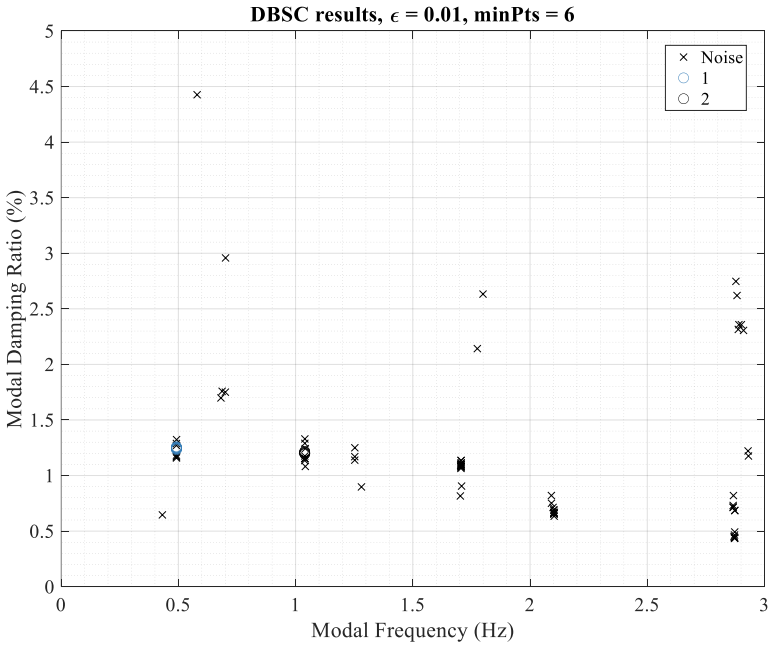

(e)

Figure 2.6. DBSCAN results with varying ϵ

Table 2.5. Modal damping ratios obtained with varying ϵ values

ϵ	Modal Damping Ratios (%)		
	V-1	**V-3**	**V-5**
0.3	1.246	N/A	1.085
0.2	1.246	1.198	1.096
0.1	1.246	1.198	1.096
0.05	1.246	1.198	1.096
0.01	1.246	1.206	N/A

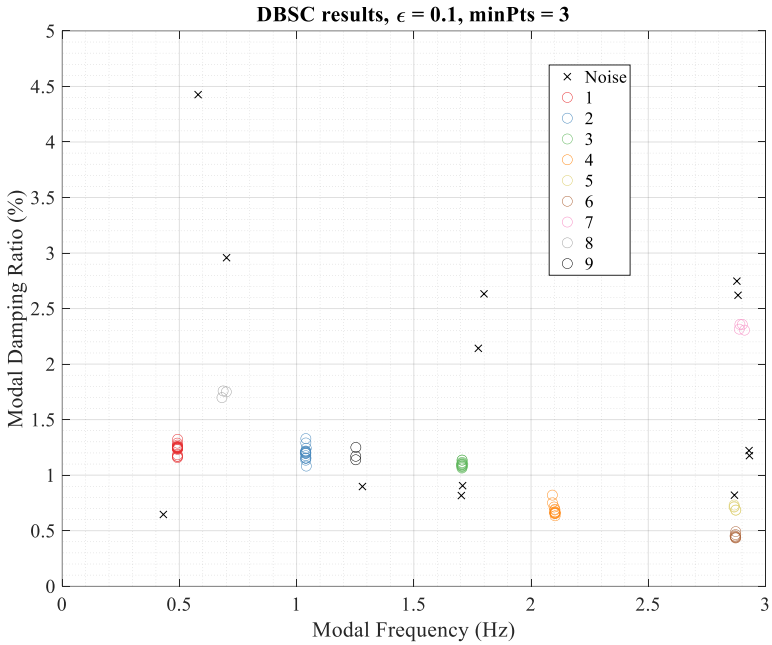
DBSC results, ϵ = 0.1, minPts = 3
Modal Damping Ratio (%)
Modal Frequency (Hz)
Noise
1
2
3
4
5
6
7
8
9

(a)

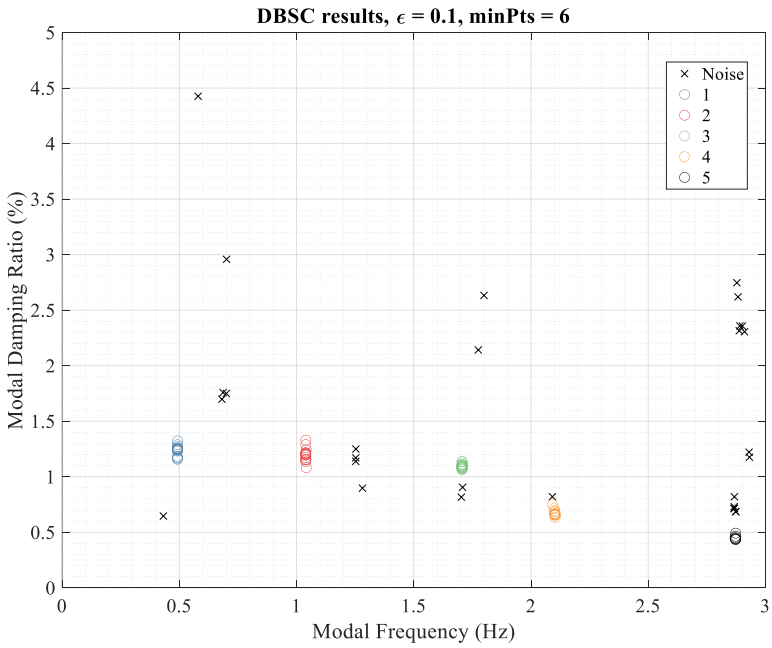
DBSC results, ϵ = 0.1, minPts = 6
Modal Damping Ratio (%)
Modal Frequency (Hz)
Noise
1
2
3
4
5

(b)

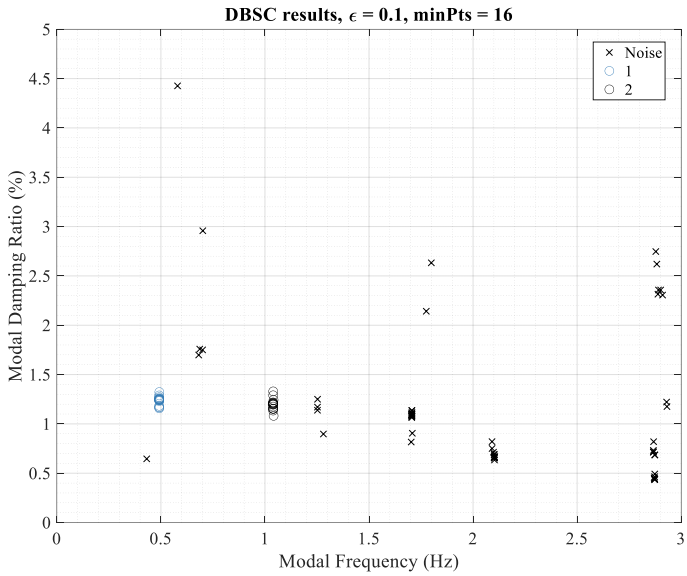

(c)

Figure 2.7. DBSCAN results with varying *minPts*

Table 2.6. Modal damping ratios obtained with varying *minPts* values

minPts	**Modal Damping Ratios (%)**		
	V-1	**V-3**	**V-5**
4~13	1.246	1.198	1.096
14~16	1.246	1.039	N/A
17	1.246	N/A	N/A

After identifying physical pole clusters from DBSCAN, clusters within predefined interested frequency ranges are selected for processing. This is done by peak-picking interested modal frequencies from PSD and finding clusters within the frequency ranges between $\pm 5\%$ of each peak-picked frequency.

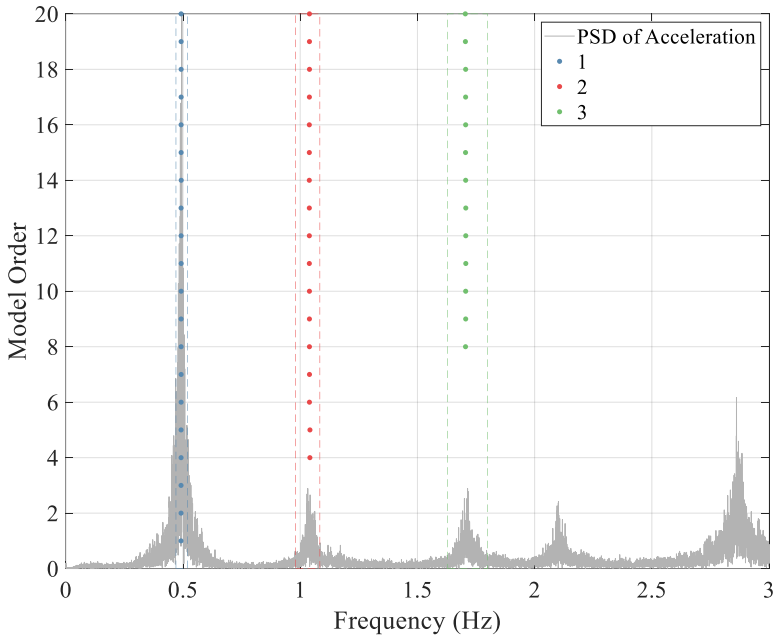

Figure 2.8. Selection of clusters for interested modes

Even after density-based clustering, it is possible that some spurious poles may still remain in the identified clusters. As a final outlier removal process, outliers outside 1.5 times the interquartile ranges are removed, as suggested in a previous study.[27] The final results of postprocessing are shown in Figure 2.9, where it is shown that damping estimates are stable with even low model orders.

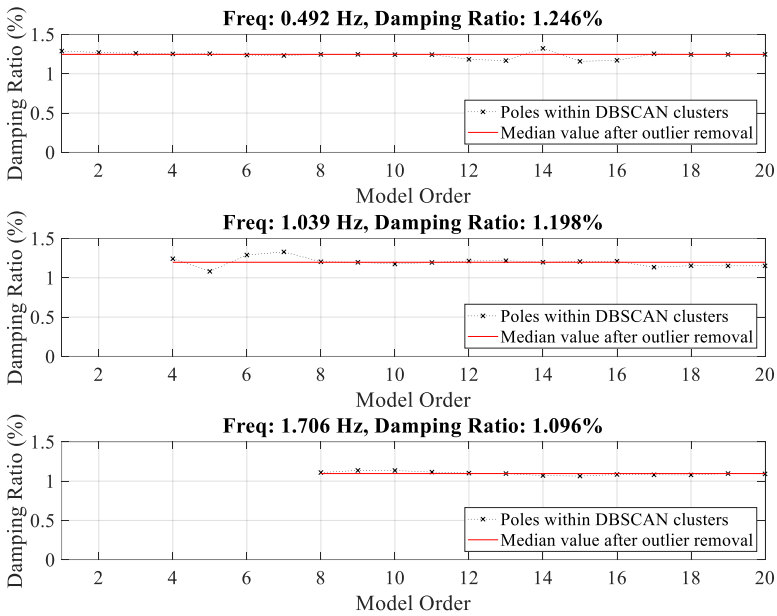

Figure 2.9. Final estimated damping ratios after outlier removal

2.4. Validation of Proposed Process

2.4.1. Numerical Validation

A numerical simulation of a 6-story shear building was performed for the developed automated damping estimation procedure. The 6-story shear building possessed an inter-story stiffness of 4000 kN and floor mass of 2,549.29 kg. Damping was configured to follow a classical damping model and the resulting modal parameters are outlined in Table 2.7. All parameters for the procedure were applied as described in the previous subchapters.

Table 2.7. Modal parameters of the numerical 6-story shear building

Mode	Modal Frequencies (Hz)	Modal Damping Ratios (%)
Mode 1	0.485	0.339
Mode 2	1.428	0.310
Mode 3	2.287	0.408
Mode 4	3.014	0.507
Mode 5	3.565	0.585
Mode 6	3.909	0.635

The shear building was subjected to white Gaussian noise excitation at the base for the duration of 1 hour and the response was calculated with a time step of 0.01 seconds. The simulation was repeated 100 times and damping ratios were estimated for the first three modes. The results are found to be quite close to the exact damping ratios. (Table 2.8) It is also confirmed here that using reconstructed displacement enhances the damping estimation results. (Table 2.9)

Table 2.8. Estimated damping ratios from numerical simulation

Mode	Exact Damping Ratio (%)	Estimated Damping Ratios	
		Mean (%)	C.O.V.
Mode 1	0.339	0.356	0.216
Mode 2	0.310	0.310	0.117
Mode 3	0.408	0.421	0.133

Table 2.9. Comparison of damping estimation results depending on utilization of reconstructed displacement

Mode	Estimated Damping Ratios			
	Reconstructed Displacement		Acceleration	
	Mean (%)	C.O.V.	Mean (%)	C.O.V.
Mode 1	0.356	0.216	0.358	0.220
Mode 2	0.310	0.117	0.303	0.161
Mode 3	0.421	0.133	0.431	0.229

2.4.2. Experimental Validation

The developed procedure was also applied to short-term operational data acquired from one of the target structures, Jindo Bridge. Data collected during summer (2017-07-22 ~ 2017-07-28) and winter (2018-02-19 ~ 2018-02-25) were selected as test datasets. Because no experimental vibration tests were performed for Jindo Bridge, damping estimates from a previous study were used to compare the results. It is found that the damping estimates of the first vertical mode from experimental validation are within the expected range of damping values from the previous study.

Table 2.10. Damping estimation results for experimental validation

Data		Mean (%)	C.O.V.
Experimental Validation Datasets	Summer	0.435	0.560
	Winter	0.705	0.604
	Total	0.577	0.652
Kim et al. [3]		0.54 ~ 0.63	N/A

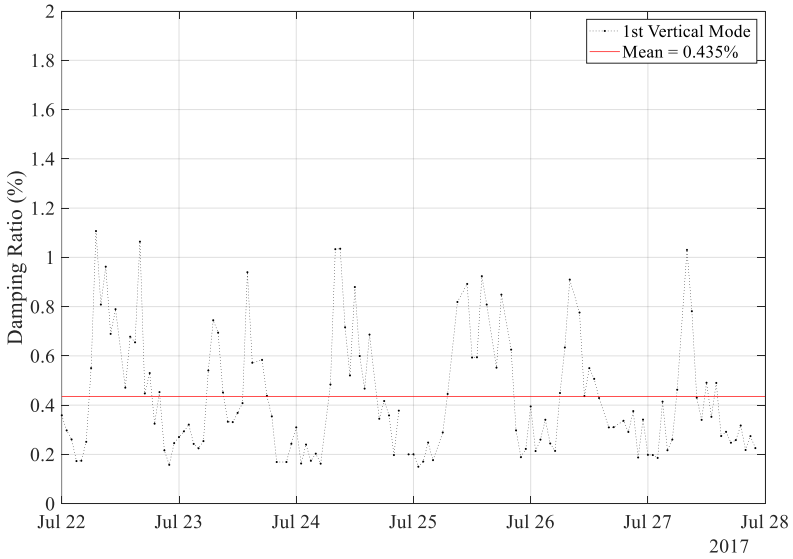

(a)

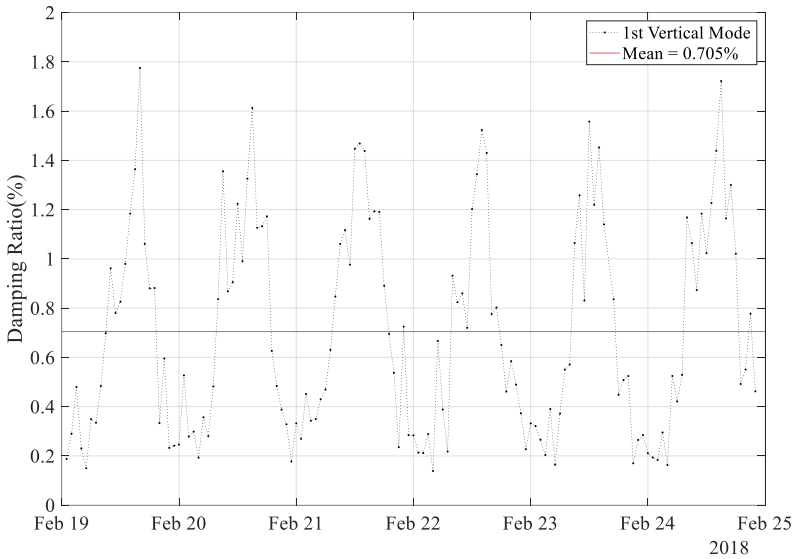

(b)

Figure 2.10. Damping estimation results for experimental validation
(a) Summer (2017-07-22 ~ 2017-07-28)
(b) Winter (2018-02-19 ~ 2018-02-25)

3. Damping Estimation from Long-Term Data

3.1. Observed Phenomena from Long-Term Data

3.1.1. VIVs at Jindo Bridge

It is already known from multiple reports that the Second Jindo Bridge was subjected to VIVs with levels exceeding serviceability limits before the installation of multiple tuned mass dampers (MTMD) in 2012.[3], [11] During examination of long-term damping estimation results for the Jindo Bridge, vibrations exceeding serviceability limits suspected to be from VIVs for the Jindo Bridge were also discovered. When the hourly mean wind direction was northwest and the hourly mean wind speed was between approximately 12~16 m/s, the first vertical mode frequency of the Jindo Bridge decreased significantly, from a mean value of 0.496 Hz to 0.486 Hz. (Figure 3.1) Furthermore, damping during such conditions were lower than what was expected for the level of excitation (Figure 3.2). These environmental conditions match the VIV conditions for Jindo Bridge predicted by Park [28], in which VIV was discovered to occur at the Jindo Bridge when the wind direction was northwest (when the Jindo Bridge was at downstream from the Second Jindo Bridge) at wind speeds of 12.2~16 m/s. With the presence of vortex-shedding forces during lock-in range, the existence of sinusoidal forces introduces a violation to the fundamental assumption of NExT and render the estimated damping ratios unreliable. Thus, damping estimate results during VIV conditions must be removed. In this study, VIV conditions are defined as when any 10-minute segment of a 1-hour data has a mean wind direction between 100°~150°, i.e. northwest (0° as North, measured clockwise) and mean wind speed between 12.2~16 m/s.

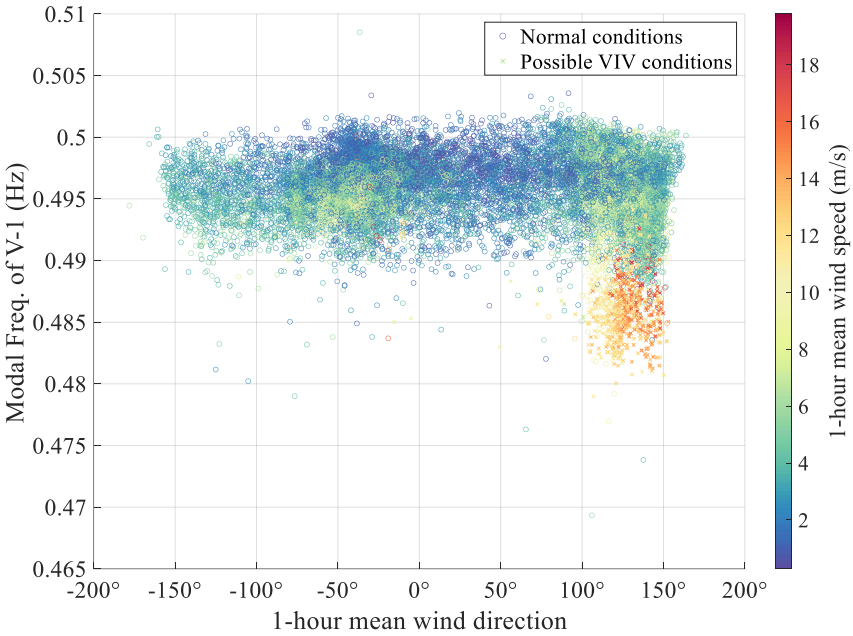

Figure 3.1. Modal frequencies of first vertical mode by wind direction

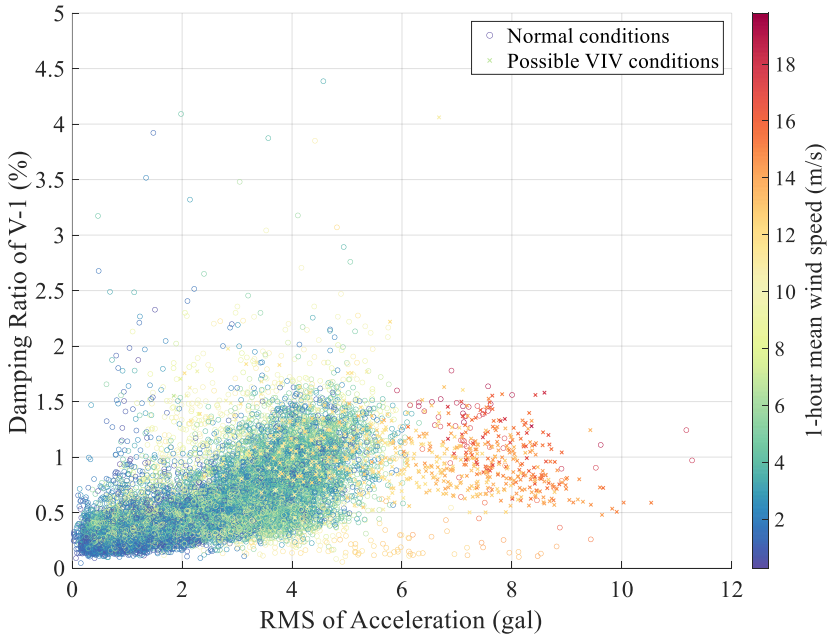

Figure 3.2. Relatively low damping ratios during VIV conditions

3.1.2. High Damping Ratios During Typhoon Conditions

Sorok Bridge was subjected to high wind conditions during Typhoon Soulik on August 23rd, 2018. Because traffic was restricted due to the passage of the typhoon, it can be understood that the main source of excitation for the bridge was wind for the duration. As Typhoon Soulik approached Sorok Bridge, high damping ratios for the first vertical mode ranging from 1.6% ~ 2.1% were estimated.

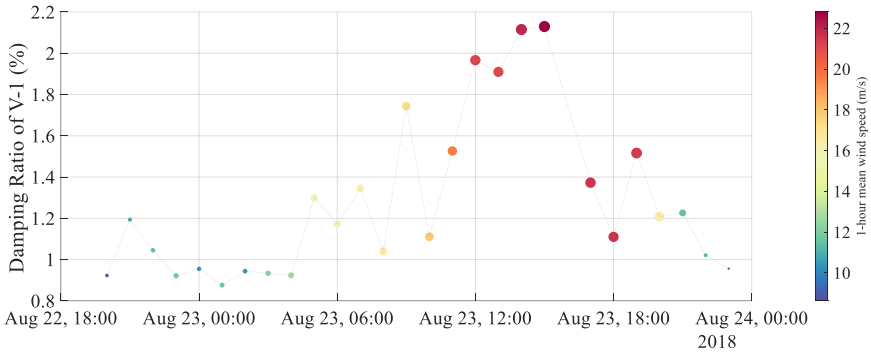

(a)

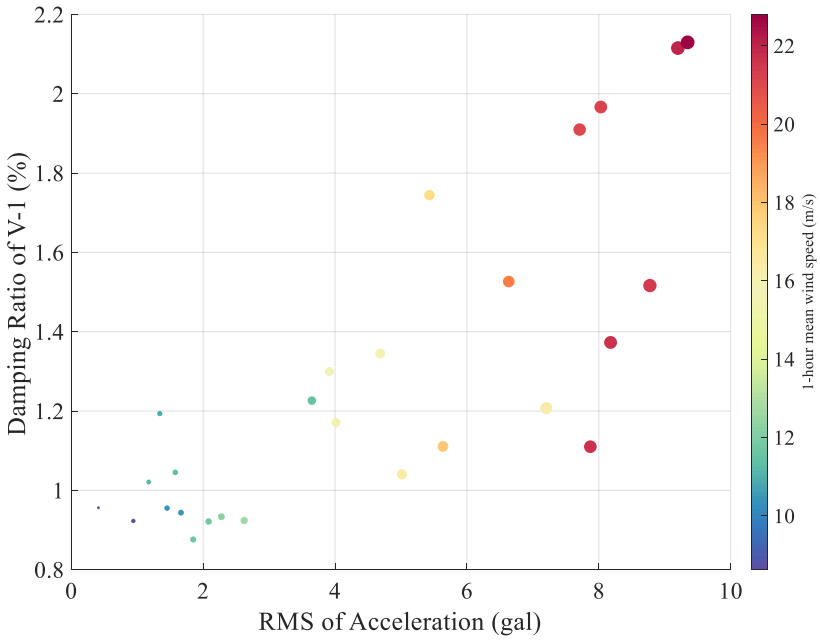

(b)

Figure 3.3. Damping estimates for Sorok Bridge during typhoon conditions (plot point size reflects RMS of acceleration for 1-hour duration)

Without flutter coefficients, it is not possible to accurately assess and remove the effects of aerodynamic damping from estimated damping ratios. Thus, it is advisable to remove datasets with such high wind conditions to accurately evaluate structural damping. Previous studies on large wind-sensitive structures have also evaluated damping for conditions in which hourly mean wind speeds were low to remove aerodynamic effects. (Under 5 m/s in [29], [30].)

3.2. Statistical Analysis

3.2.1. Environmental Effects on Damping Ratios

To accurately evaluate structural damping, the following criteria were used to remove aerodynamic effects and operational conditions with insufficient excitation. VIV conditions for Jindo Bridge are included in the first criterion. (Table 3.1)

Table 3.1. Removal of suboptimal environmental conditions

Conditions	Criteria	Value
High wind speed conditions	Maximum 10-minute mean wind speed during a 1-hour period, $\max(\overline{u_{10}})$	$\max(\overline{u_{10}}) > 8$ m/s
Low excitation conditions	Maximum 10-minute RMS of acceleration during a 1-hour period, $\max(\mathrm{rms}(\mathrm{acc}))$	$\max(\mathrm{rms}(\mathrm{acc}_{10})) < 0.1$ gal

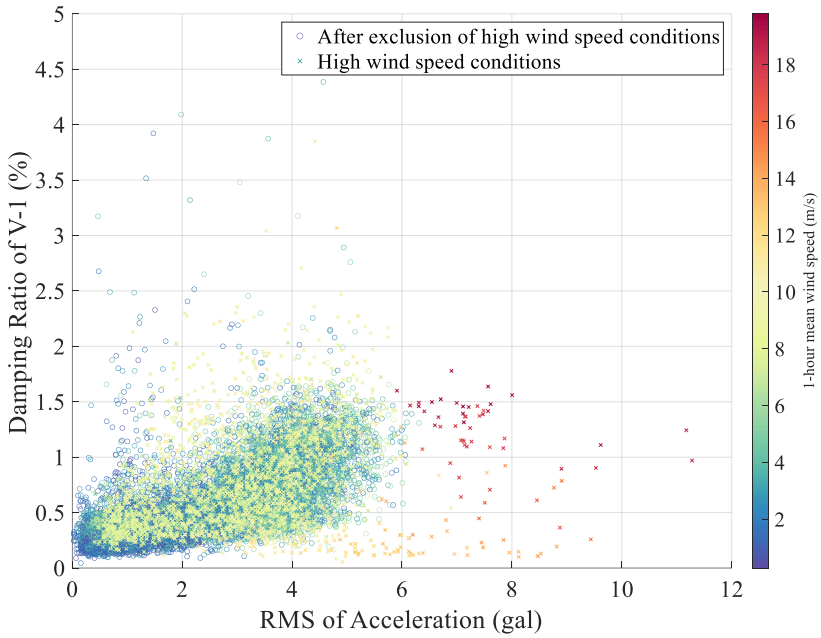

(a)

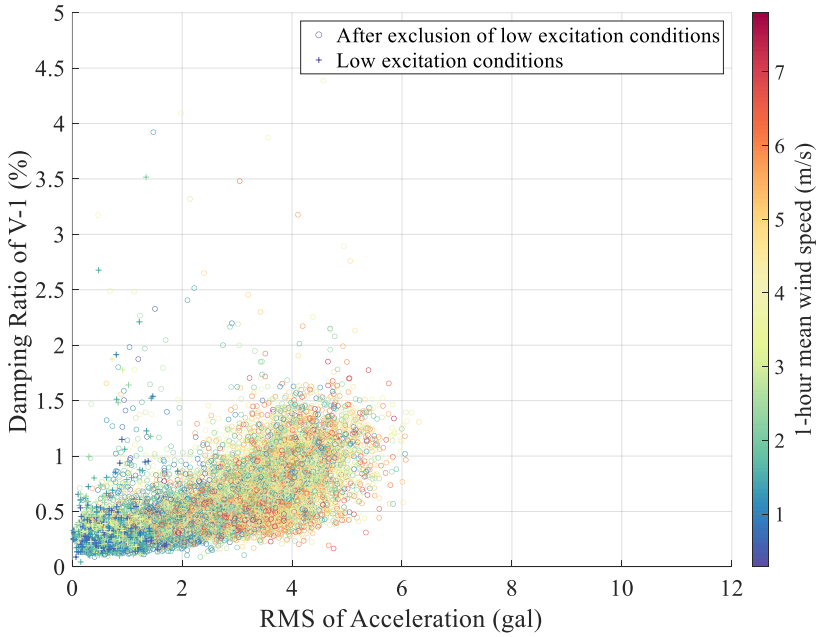

(b)

Figure 3.4. Jindo Bridge, removal of suboptimal environmental conditions

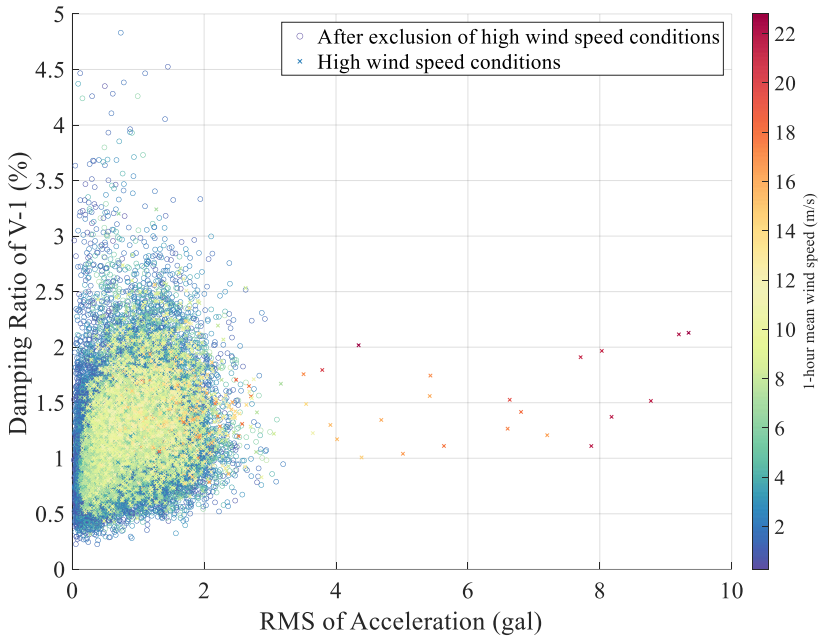

(a)

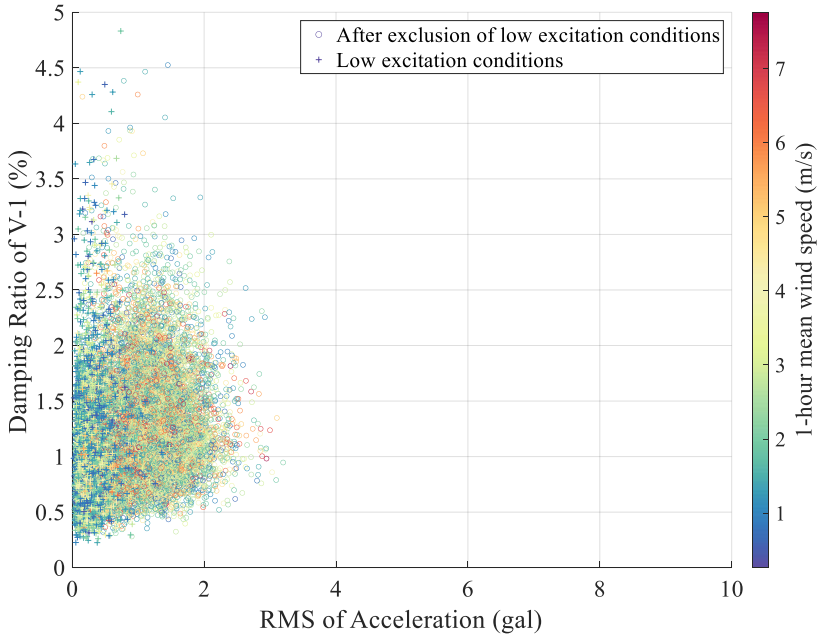

(b)

Figure 3.5. Sorok Bridge, removal of suboptimal environmental conditions

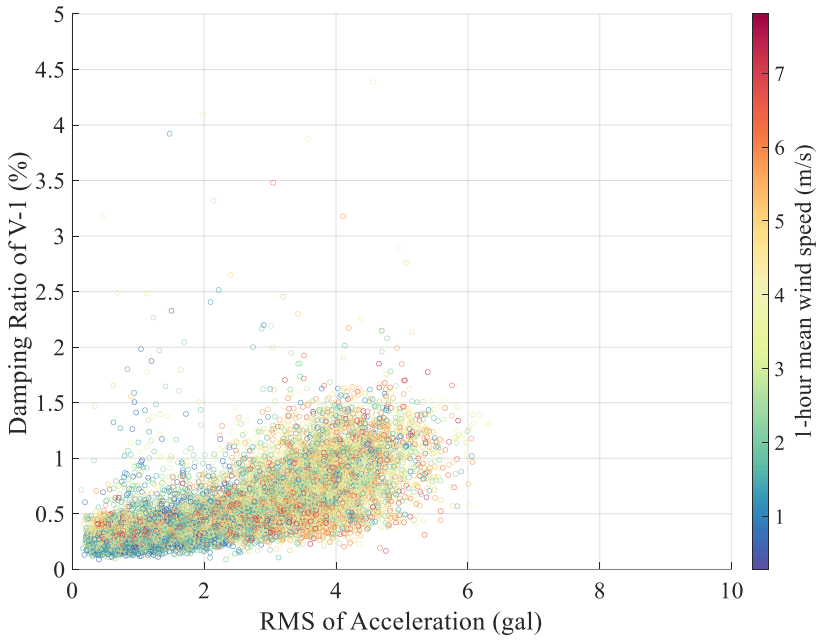

(a)

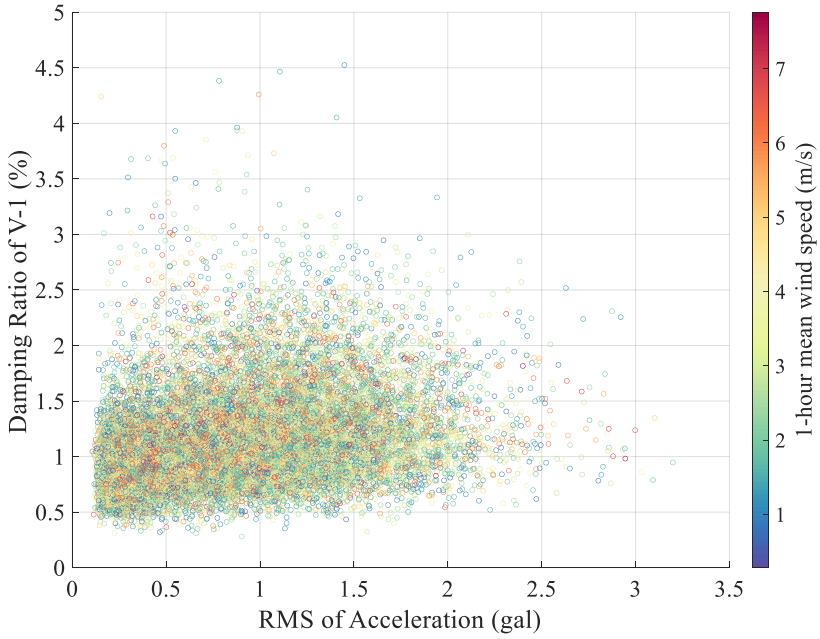

(b)

Figure 3.6. Amplitude dependency of damping ratios
(a) Jindo Bridge; (b) Sorok Bridge

By removing suboptimal environmental conditions from long-term data, amplitude dependency is better observed, especially for Jindo Bridge. While it is less observable in the Sorok Bridge, it can be observed that the level of excitation provides some baseline of damping ratios as the RMS of acceleration increases. Recommendations regarding further research on this issue is provided in subchapter 4.2.

3.2.2. Variability of Damping Ratios by Time Intervals

Variability of damping ratios by time intervals was also examined. Estimated damping ratios were grouped by hour, weekday, month and year. Box plots of each time intervals are shown below.

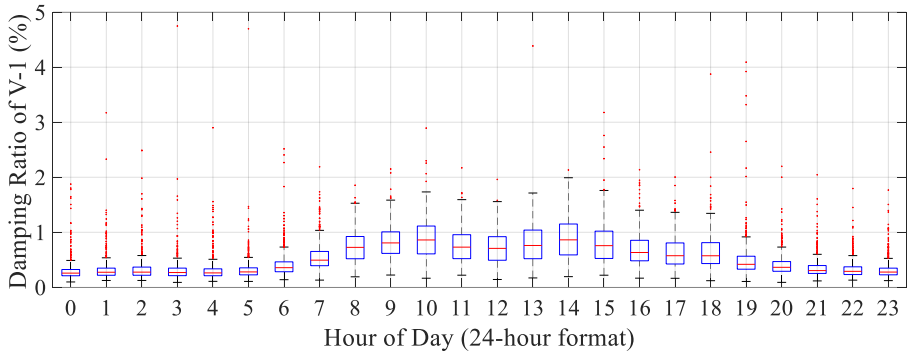

(a)

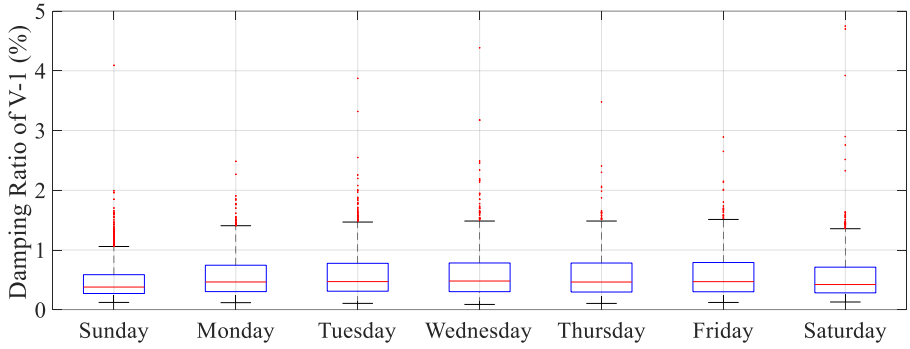

(b)

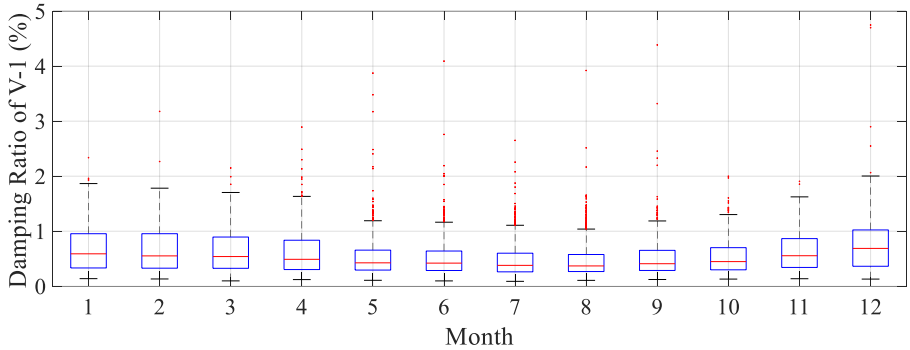

(c)

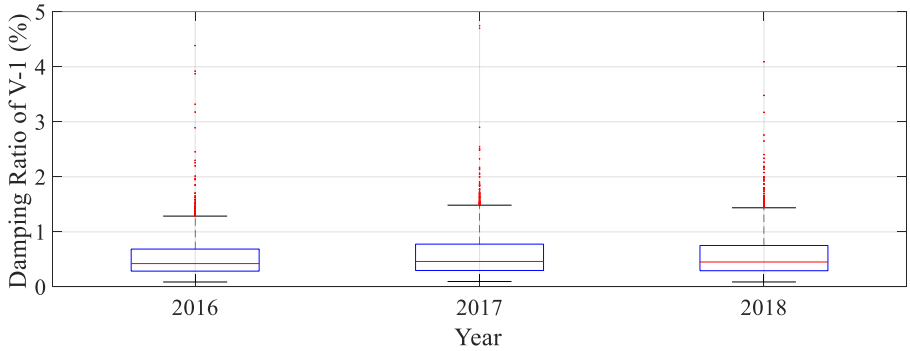

(d)

Figure 3.7. Jindo Bridge, variability of damping ratios by time intervals

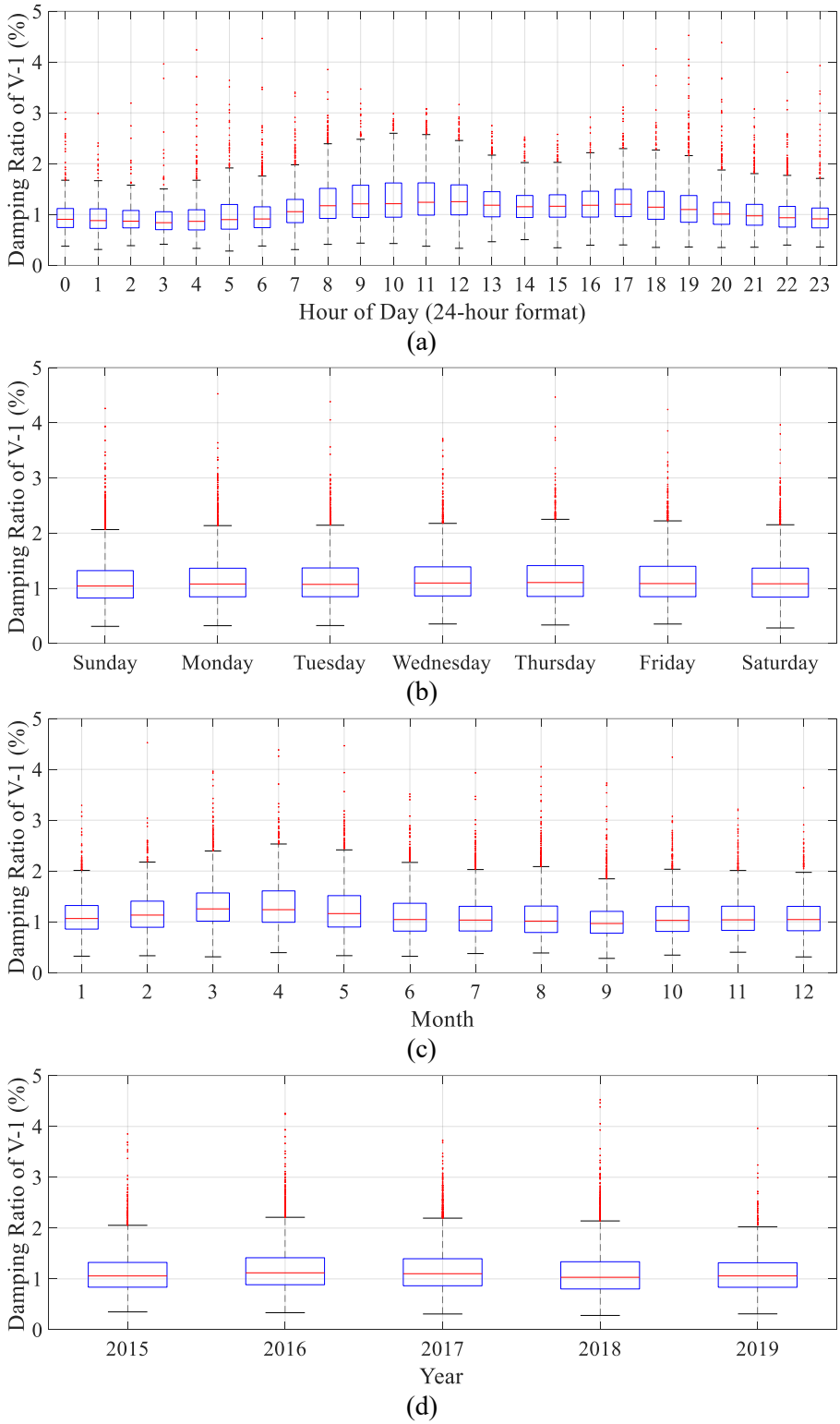

Figure 3.8. Sorok Bridge, variability of damping ratios by time intervals

For weekday, month and year, no meaningful variations could be discerned. For hourly variations however, damping ratios were noticeably higher during daytime and lower during nighttime. These hourly variations in damping ratios may be linked to change in traffic volume, as aerodynamic effects were removed beforehand. While there were no long-term weigh-in-motion (WIM) system data for either of the target structures, annual traffic reports for some National Routes exist, in which year-round hourly traffic is recorded. Jindo Bridge is a part of National Route 18, connecting Jindo-eup and Munnae-myeon. Sorok Bridge is a part of National Route 27, connecting Geumsan-myeon and Doyang-eup. Fortunately, both bridges were monitored by automatic vehicle classification (AVC) instruments, and year-long hourly traffic data was acquired from an online database provided by the Korean Institute of Construction Technology (KICT).[31]

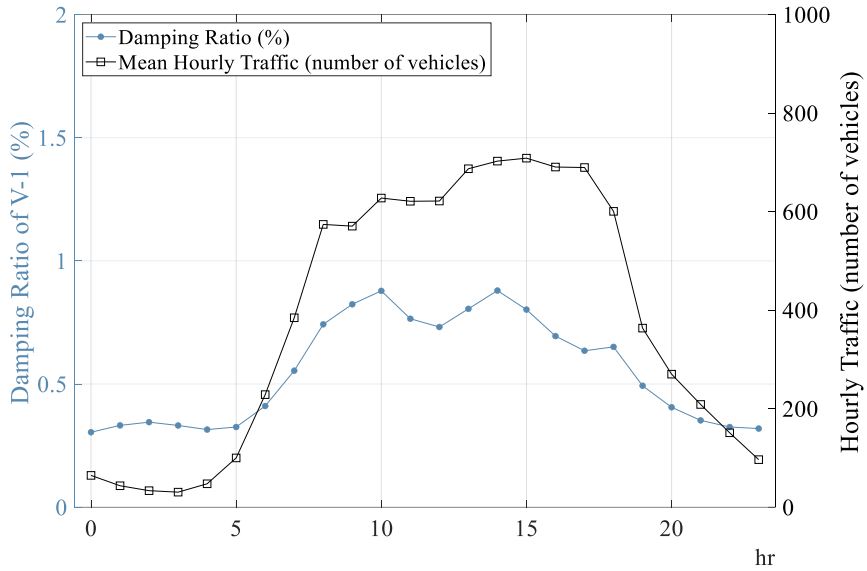

(a)

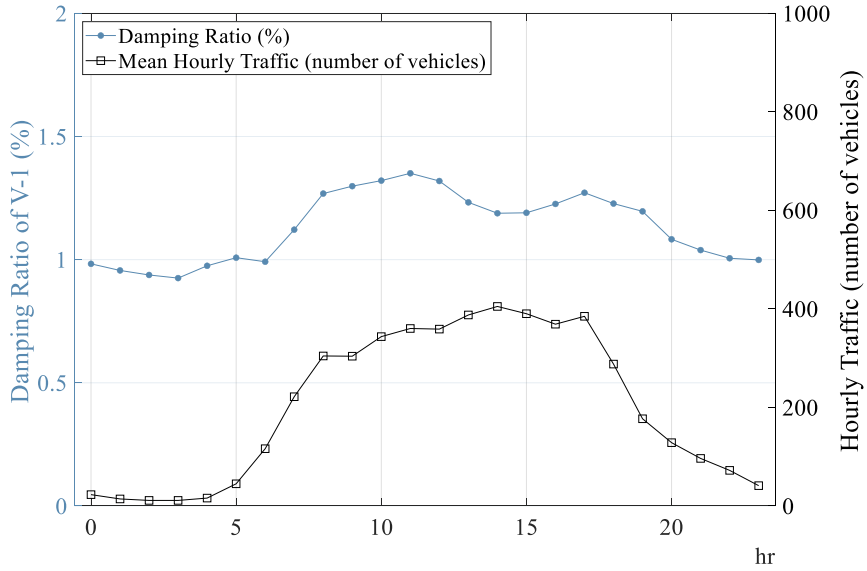

(b)

Figure 3.9. Mean hourly damping ratios and mean hourly traffic (a) Jindo Bridge; (b) Sorok Bridge

3.2.3. Statistical Models of Damping Ratios

In this study, several distribution types are considered through goodness-of-fit to identify the distribution that best reflects damping ratios.

Before comparing goodness-of-fit measure values, it is important to select reasonable candidate distributions. Most previous studies have considered lognormal or log-logistics distributions for damping ratios and thus are included in the candidate distributions.[9] Other distributions such as normal, exponential, gamma, logistic, Rayleigh, beta and Weibull are also included.

Akaike Information Criterion (AIC) is often used to measure how well a statistical model fits the given data. AIC is able to consider the trade-off between goodness of fit and model interpretability, and thus is able to handle both risks of overfitting and underfitting.

For all modes, modal damping ratios best followed either lognormal or log-logistic distribution. Furthermore, differences in AIC was minimal between the two distributions. Thus, lognormal distribution was used to fit the statistical models of damping ratios.

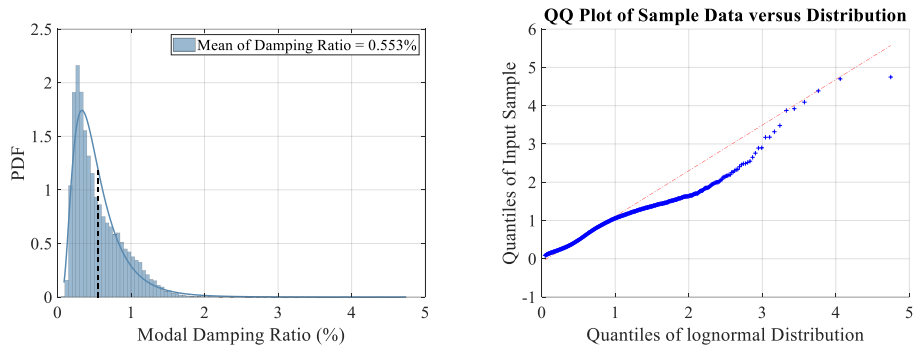

(a)

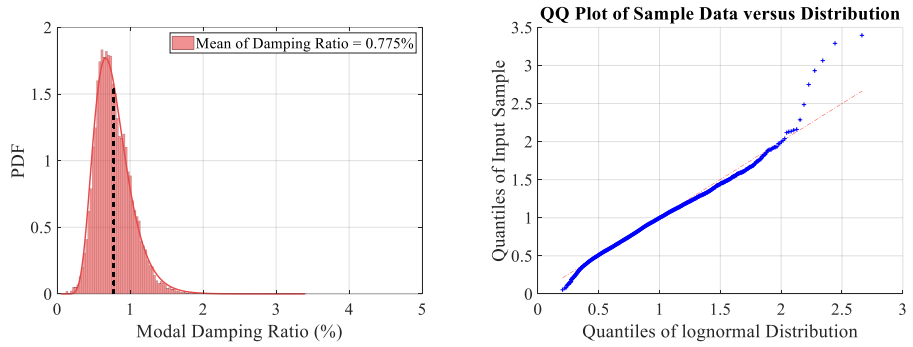

(b)

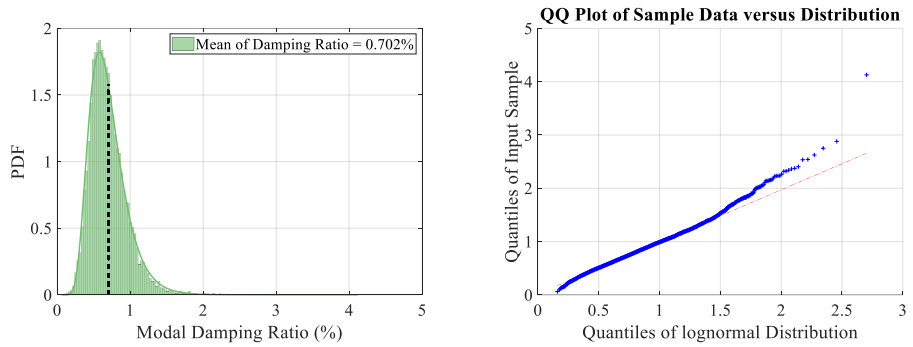

(c)

Figure 3.10. Histograms and Q-Q Plots for Jindo Bridge, (a) V-1; (b) V-3; (c) V-5

Table 3.2. Mean and distribution parameters for Jindo Bridge

Mode	Mean (%)	Distribution Parameters	
		μ	σ
V-1	0.553	-0.763	0.582
V-3	0.775	-0.305	0.322
V-5	0.702	-0.417	0.354

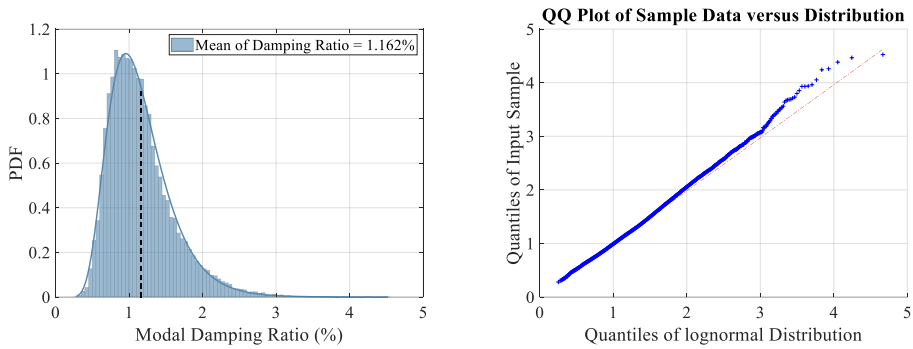

(a)

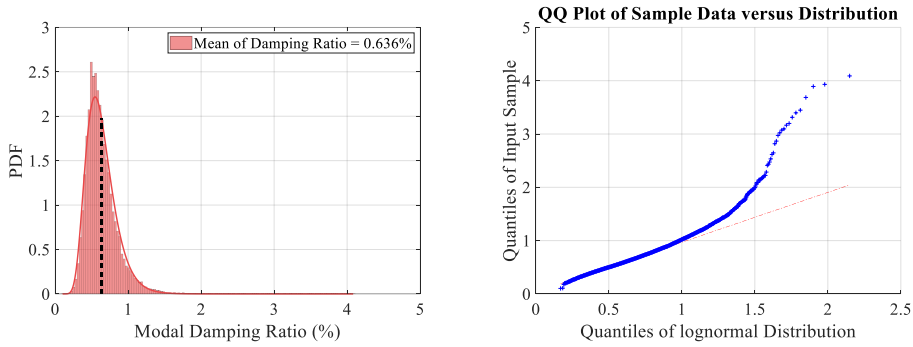

(b)

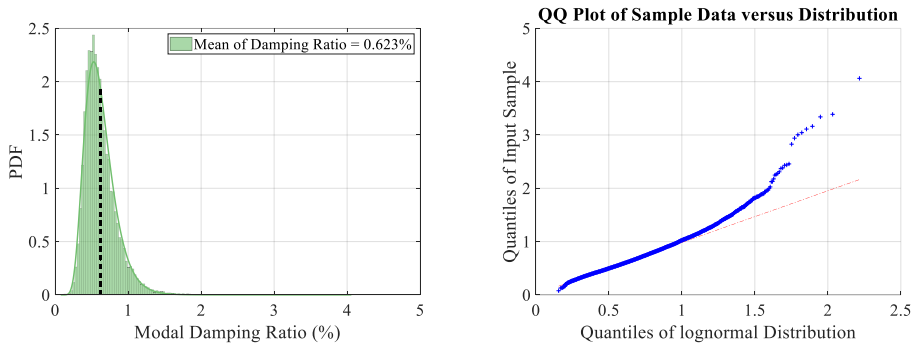

(c)

Figure 3.11. Histograms and Q-Q Plots for Sorok Bridge
(a) V-1; (b) V-3; (c) V-5

Table 3.3. Mean and distribution parameters for Sorok Bridge

Mode	Mean (%)	Distribution Parameters	
		μ	σ
V-1	1.162	0.084	0.359
V-3	0.636	-0.505	0.313
V-5	0.623	-0.530	0.327

4. Conclusions and Recommendations

4.1. Conclusions

The objectives of this dissertation were to first, develop an automated damping estimation process that is robust against faulty data and requires minimum user intervention. The second objective was to examine the environmental effects on damping ratios and construct statistical models from long-term data. The following conclusions were made based on the previous chapters.

1. The proposed automated process allowed stable damping estimation even with sparse sensors and small model order. Density-based clustering was successful in identifying physical modes while eliminating spurious poles that remained after application of hard validation criteria. Parameters for robust density-based clustering were suggested based on both physical characteristics of the structures and parametric study.

2. Using the proposed process, damping ratios for both Jindo and Sorok Bridges were evaluated to compare with the current recommended design values. Mean damping ratios of the first vertical modes for Jindo and Sorok Bridges were found to be 0.553% and 1.162%, exceeding design value of 0.4%. This is similar to damping ratios estimated by previous studies, summarized in Table 4.1.

Table 4.1. Comparison of estimated damping ratio for V-1 with previous studies

Bridge	Mode	Estimated Damping Ratio (%)	
		Current Study	Previous Studies
Jindo Bridge	V-1	0.553	0.54 ~ 0.63 ([3])
Sorok Bridge	V-1	1.162	1.1 ~ 1.5 ([32]), 0.91 ([33])

3. Amplitude dependency of damping ratio was observed for the Jindo Bridge from analysis of long-term data. Thus, when evaluating damping capacity of a structure, it must be with regards to their level of excitation.

4. Variations in damping ratios by different hours, weekdays, months and years was examined, and was found that damping was higher for hours with higher traffic volume.

4.2. Recommendations

1. Excessive vibrations greater than serviceability limits by suspected VIVs have occurred on the Jindo Bridge. Even though this phenomenon was predicted in a previous study, the installation of MTMD at the Second Jindo Bridge or perhaps changes in structural properties may have changed the conditions. Further investigation utilizing long-term data from both Jindo and the Second Jindo Bridge is recommended to assess this issue.

2. Compared to Jindo Bridge, Sorok Bridge did not display clear amplitude dependency. Additional modifications on the proposed process or field test with a dense sensor array is recommended to improve the results.

3. Damping estimation for different types of bridges can be performed in order to build a damping database. Correlation analysis with respect to various structural properties such as span length, material type and configuration can be performed to further understanding of damping in bridges.

References

[1] A. K. Chopra, *Dynamics of Structures: Theory and Applications to Earthquake Engineering*. Pearson Education Limited, 2015.

[2] 배두병, 오창국, 한국교량및구조공학회, and 교량설계핵심기술연구단, 도로교설계기준(한계상태설계법)해설. 서울: 건설정보사, 2018.

[3] S.-J. Kim, H.-K. Kim, R. Calmer, J. Park, G. S. Kim, and D. K. Lee, "Operational field monitoring of interactive vortex-induced vibrations between two parallel cable-stayed bridges," *Journal of Wind Engineering and Industrial Aerodynamics*, vol. 123, pp. 143–154, Dec. 2013, doi: 10.1016/j.jweia.2013.10.001.

[4] S. Kim, H.-K. Kim, and Y. C. Hwang, "Enhanced Damping Estimation for Cable-Stayed Bridges Based on Operational Monitoring Data," *Structural Engineering International*, vol. 28, no. 3, pp. 308–317, 2018.

[5] Y. C. Hwang, S. Kim, and H.-K. Kim, "Cause investigation of high-mode vortex-induced vibration in a long-span suspension bridge," *Structure and Infrastructure Engineering*, vol. 16, no. 1, pp. 84–93, Jan. 2020, doi: 10.1080/15732479.2019.1604771.

[6] C. Rainieri and G. Fabbrocino, *Operational Modal Analysis of Civil Engineering Structures: An Introduction and Guide for Applications*. Springer, 2014.

[7] S. Soyoz and M. Q. Feng, "Long-Term Monitoring and Identification of Bridge Structural Parameters," *Computer-Aided Civil and Infrastructure Engineering*, vol. 24, no. 2, pp. 82–92, 2009, doi: 10.1111/j.1467-8667.2008.00572.x.

[8] J.-X. Mao, H. Wang, Y.-G. Fu, and B. F. Spencer Jr, "Automated modal identification using principal component and cluster analysis: Application to a long-span cable-stayed bridge," *Structural Control and Health Monitoring*, vol. 26, no. 10, p. e2430, Oct. 2019, doi: 10.1002/stc.2430.

[9] Asadollahi Parisa and Li Jian, "Statistical Analysis of Modal Properties of a Cable-Stayed Bridge through Long-Term Wireless Structural Health Monitoring," *Journal of Bridge Engineering*, vol. 22, no. 9, p. 04017051, Sep. 2017, doi: 10.1061/(ASCE)BE.1943-5592.0001093.

[10] Zhang Yilan, Kurata Masahiro, and Lynch Jerome P., "Long-Term Modal Analysis of Wireless Structural Monitoring Data from a Suspension Bridge under Varying Environmental and Operational Conditions: System Design and Automated Modal Analysis," *Journal of Engineering Mechanics*, vol. 143, no. 4, p. 04016124, Apr. 2017, doi: 10.1061/(ASCE)EM.1943-7889.0001198.

[11] S. Kim, J. Park, and H.-K. Kim, "Damping identification and serviceability assessment of a cable-stayed bridge based on operational

monitoring data," *Journal of Bridge Engineering*, vol. 22, no. 3, p. 04016123, 2016.

[12] R. L. Boroschek and J. A. Bilbao, "Interpretation of stabilization diagrams using density-based clustering algorithm," *Engineering Structures*, vol. 178, pp. 245–257, Jan. 2019, doi: 10.1016/j.engstruct.2018.09.091.

[13] S. Kim, K.-Y. Park, H.-K. Kim, and H. S. Lee, "Damping estimates from reconstructed displacement for low-frequency dominant structures," *Mechanical Systems and Signal Processing*, vol. 136, p. 106533, Feb. 2020, doi: 10.1016/j.ymssp.2019.106533.

[14] Y. H. Hong, H.-K. Kim, and H. S. Lee, "Reconstruction of dynamic displacement and velocity from measured accelerations using the variational statement of an inverse problem," *Journal of Sound and Vibration*, vol. 329, no. 23, pp. 4980–5003, Nov. 2010, doi: 10.1016/j.jsv.2010.05.016.

[15] G. H. James, T. G. Carne, J. P. Lauffer, and A. R. Nord, "Modal testing using natural excitation," in *Proceedings of the International Modal Analysis Conference*, 1992, pp. 1208–1208.

[16] Nayeri Reza D. *et al.*, "Study of Time-Domain Techniques for Modal Parameter Identification of a Long Suspension Bridge with Dense Sensor Arrays," *Journal of Engineering Mechanics*, vol. 135, no. 7, pp. 669–683, Jul. 2009, doi: 10.1061/(ASCE)0733-9399(2009)135:7(669).

[17] J. S. Bendat and A. G. Piersol, *Random data: analysis and measurement procedures*. Wiley, 2000.

[18] 김선중, "Enhancing damping estimation in cable-supported bridges under operational conditions," PhD Thesis, 서울대학교 대학원, 2017.

[19] J. M. Caicedo, "PRACTICAL GUIDELINES FOR THE NATURAL EXCITATION TECHNIQUE (NExT) AND THE EIGENSYSTEM REALIZATION ALGORITHM (ERA) FOR MODAL IDENTIFICATION USING AMBIENT VIBRATION," *Experimental Techniques*, vol. 35, no. 4, pp. 52–58, 2011, doi: 10.1111/j.1747-1567.2010.00643.x.

[20] J.-N. JUANG and R. S. PAPPA, "An eigensystem realization algorithm for modal parameter identification and model reduction," *Journal of Guidance, Control, and Dynamics*, vol. 8, no. 5, pp. 620–627, 1985, doi: 10.2514/3.20031.

[21] G. J. Yun, S.-G. Lee, and S. Shang, "An improved mode accuracy indicator for Eigensystem Realization Analysis (ERA) techniques," *KSCE J Civ Eng*, vol. 16, no. 3, pp. 377–387, Mar. 2012, doi: 10.1007/s12205-012-1236-y.

[22] C. Rainieri and G. Fabbrocino, "Development and validation of an automated operational modal analysis algorithm for vibration-based monitoring and tensile load estimation," *Mechanical Systems and Signal Processing*, vol. 60–61, pp. 512–534, Aug. 2015, doi: 10.1016/j.ymssp.2015.01.019.

[23] M. Ester, H.-P. Kriegel, J. Sander, and X. Xu, “A density-based algorithm for discovering clusters in large spatial databases with noise.,” in *Kdd*, 1996, vol. 96, pp. 226–231.

[24] “Density-based spatial clustering of applications with noise (DBSCAN) - MATLAB dbscan.” [Online]. Available: https://www.mathworks.com/help/stats/dbscan.html#mw_d5194229-d5e8-4f30-8fa4-5f241315846e. [Accessed: 26-Jan-2020].

[25] J. Sander, M. Ester, H.-P. Kriegel, and X. Xu, “Density-Based Clustering in Spatial Databases: The Algorithm GDBSCAN and Its Applications,” *Data Mining and Knowledge Discovery*, vol. 2, no. 2, pp. 169–194, Jun. 1998, doi: 10.1023/A:1009745219419.

[26] E. Schubert, J. Sander, M. Ester, H. P. Kriegel, and X. Xu, “DBSCAN Revisited, Revisited: Why and How You Should (Still) Use DBSCAN,” *ACM Trans. Database Syst.*, vol. 42, no. 3, pp. 19:1–19:21, Jul. 2017, doi: 10.1145/3068335.

[27] F. Magalhães, Á. Cunha, and E. Caetano, “Online automatic identification of the modal parameters of a long span arch bridge,” *Mechanical Systems and Signal Processing*, vol. 23, no. 2, pp. 316–329, Feb. 2009, doi: 10.1016/j.ymssp.2008.05.003.

[28] J. Park, “Vortex-induced Vibration Generated by Flow Interaction between Two Cable-stayed Bridges in Tandem,” PhD Thesis, 서울대학교 대학원, 2016.

[29] E. Cheynet, J. B. Jakobsen, and J. Snæbjörnsson, “Damping estimation of large wind-sensitive structures,” *Procedia Engineering*, vol. 199, pp. 2047–2053, Jan. 2017, doi: 10.1016/j.proeng.2017.09.471.

[30] E. Cheynet, J. Snæbjörnsson, and J. Jakobsen, “Identifying Traffic-Induced Vibrations of a Suspension Bridge: A Modelling Approach Based on Full-Scale Data,” 2020, pp. 93–101.

[31] “⊙ 교통량정보제공 시스템 ⊙.” [Online]. Available: http://www.road.re.kr/main/main.asp. [Accessed: 28-Jan-2020].

[32] 박동욱 and 김남식, “확장형 칼만필터를 이용한 현수교의 감쇠성능 평가,” *대한토목학회논문집 A*, vol. 31, no. 2A, pp. 89–96, 2011.

[33] S. Kim and H.-K. Kim, “Damping Identification of Bridges Under Nonstationary Ambient Vibration,” *Engineering*, vol. 3, no. 6, pp. 839–844, Dec. 2017, doi: 10.1016/j.eng.2017.11.002.

국 문 초 록

본 연구에서는 장기 데이터를 통한 케이블 교량의 감쇠 평가를 위한 과정을 제시한다. 장대 케이블 교량은 상대적으로 유연하고 낮은 감쇠를 가지고 있기 때문에, 진동 사용성 평가를 수행 시 감쇠비는 중요한 변수가 된다. 현재까지 단기 계측 데이터를 활용하는 감쇠비 추정 및 평가에 대한 많은 기여와 관심이 있었지만, 장기적으로 환경 요인에 영향으로 인한 감쇠비의 변동성에 대해서는 아직 많은 연구가 이루어지지 않았고, 밝혀진 바가 적다. 이에 대한 연구를 수행하기 위해서 두 케이블 교량의 계측 시스템으로부터 장기 운용 데이터를 취득하였다. Natural Excitation Technique – Eigensystem Realization Algorithm (NExT-ERA)에 기반한, 밀도 기반 클러스터링 알고리즘을 사용하는 자동화된 감쇠비 추정 과정을 제시하여 사용자 개입을 최소화하였다. 이를 통하여 안정적으로 장기 데이터로부터 감쇠비를 추정할 수 있었고, 감쇠비의 진폭 의존도 (amplitude dependency) 및 공기역학적 현상에 의한 영향을 확인할 수 있었다. 여러 환경 요인을 고려하여 감쇠비를 평가하였고, 이에 따른 통계적 모델을 제시하였다. 추후 유사한 연구를 다양한 케이블 교량에 적용함으로써 감쇠비 데이터베이스를 구축할 수 있을 것으로 기대된다.

주요어: 자동화 응답기반모드해석, 케이블 교량, 감쇠, 장기 계측 데이터, NExT-ERA

학번: 2018-22388